EES Catalysis

Accepted Manuscript

This article can be cited before page numbers have been issued, to do this please use: M. Afshari, A. Hassan, A. Refaie, S. Shakoorian, P. Aleta and M. Rahimi, *EES Catal.*, 2026, DOI: 10.1039/D6EY00122J.

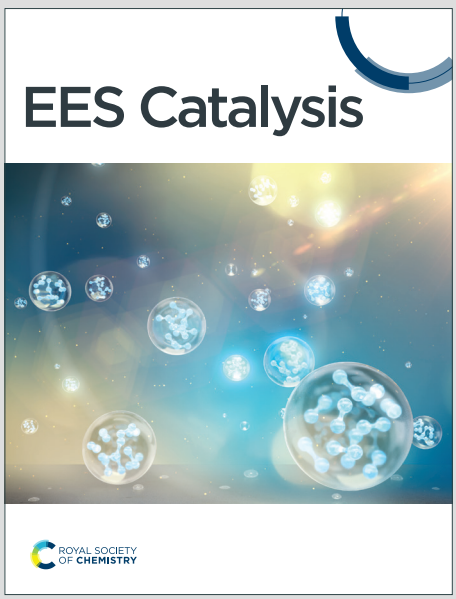

View Article Online
DOI: 10.1039/D6EY00122J

Carbon capture, utilization, and storage (CCUS) is central to carbon management, but conventional thermally driven approaches are energy-intensive and impractical. Electrochemical CO_2 separation and electroreduction are promising yet mostly remain at lab scales. In the sequential approach, separation is capital-intensive and requires energy for CO2 desorption with no added value, while electroreduction relies on purified CO_2 feedstock and cannot process dilute sources such as flue gas or air. Integrating both as reactive carbon capture (RCC) could reduce energy and costs, but introduces coupled electrochemical, catalytic, system-level, and techno-economic complexities.

To clarify the state of the field, we analyzed nearly all published RCC studies with select sequential counterparts and compiled key performance metrics. Benchmarking shows RCC has achieved lower production rates (partial current densities) than sequential systems. Within RCC, (bi)carbonate media generally outperform other chemistries. We also show that alkalinity regeneration, as an inherent RCC feature, has been largely overlooked and depends on CO_2RR product type and single-pass conversion ratio. Furthermore, TEA indicates CO is the most viable near-term product. Finally, we highlight three priorities: alkalinity regeneration, microenvironments engineering guided by multiscale modeling to boost partial current density, and assessing catalyst and device level durability under realistic operating conditions.

View Article Online
DOI: 10.1039/D6EY00122J

Electrochemical Reactive Carbon Capture: What Has Been Achieved and What Remains to Be Explored

Mohsen Afshari[1], Ahmad Hassan[1], Abdelrahman Refaie[1], Sheida Shakoorian[1], Prince Aleta[1], Mim Rahimi[1,2,*]

[1] Department of Civil and Environmental Engineering, University of Houston, Houston, TX 77204, USA
[2] Materials Science and Engineering Program, University of Houston, Houston, TX 77204, USA
* Corresponding author: mrahimi@uh.edu

ABSTRACT

Electrochemical reactive carbon capture (RCC) integrates CO_2 separation and conversion within a single process, offering a potential reduction in energy and process complexity compared to the conventional sequential route for CO_2 reduction reaction (CO_2RR). Here, we provided a comprehensive analysis of RCC spanning energetics, mechanistic understanding, electrochemical benchmarking, and unanswered key questions for advancement. While in principle RCC can reduce energy consumption by up to ~40% relative to sequential CO_2RR by bypassing desorption and compression, experimental systems currently deliver smaller gains due to higher cell voltages and lower partial current densities. Benchmarking over one hundred studies revealed that in similar voltage ranges, RCC typically achieves partial current densities of ~200 mA/cm^2, well below >1,000 mA/cm^2 in gas-fed sequential electrolyzers. Among capture media, (bi)carbonate-based systems outperform carbamate systems in both partial current density and cell voltage in ambient temperature and pressure, likely due to their easier release of in situ CO_2 (*i*-CO_2) upon protonation and absence of large ammonium cations increasing the electrical double layer thickness. Techno-economic analyses confirmed that RCC is near cost parity with sequential systems for CO and ethylene (C_2H_4), whereas liquid products remain unfeasible due to the energy-intensive downstream liquid-phase product separation. To advance RCC, we identified three research domains that remain to be explored. First, RCC studies have largely overlooked the system-level (i.e., holistic) perspective, with alkalinity regeneration often neglected while most efforts focused narrowly on CO_2RR metrics. We demonstrated that this concept heavily depends on CO_2RR product type and the single-pass conversion ratio, which has been a central metric in sequential CO_2RR research. Second, achieving high partial current densities remains challenging due to (i) limited *i*-CO_2 transport to catalyst interface and (ii) exhaustion of the already limited *i*-CO_2 by the generated hydroxides from CO_2RR and parasitic hydrogen evolution. To resolve these two issues, we proposed control of microenvironment, e.g. optimizing the hierarchial porosity or utilizing redox-active neucleophile coatings, guided by multi-scale modeling as the key research priority. Finally, long-term stability, across catalyst and device scales, has not been comprehensively studied. We highlighted the necessity of descriptors for catalyst stability and prolonged experiments for diagnosis and improvement of device stability.

Keywords: CO_2 Upgrade; CO_2RR; Reactive Carbon Capture; TEA; System Benchmarking; Microenvironment; Multi-scale Modeling

View Article Online
DOI: 10.1039/D6EY00122J

1. INTRODUCTION

The upgrading of carbon dioxide (CO_2) into value-added chemicals offers a viable route to simultaneously mitigate greenhouse gas emissions and provide sustainable carbon feedstocks for chemical manufacturing [1,2]. Various upgrading approaches, including biochemical [3], electrochemical [4,5], photochemical [6,7], and thermochemical [8,9] methods, have been proposed and extensively investigated in the past decades to produce value-added chemicals from CO_2. Among these, electrochemical CO_2 upgrading is particularly appealing due to its relatively high process efficiency, low operational temperature and pressure, controllable selectivity, and potential for industrial applications [4,10]. When coupled with a renewable energy source such as wind or solar, electrochemical processes could potentially result in generating low-carbon-emission products. Additionally, such a process can be a convenient way to store renewable energy in chemical form, acting as an energy storage system [5]. The stored energy can be released later for end-use by oxidizing the chemicals (e.g., fuels) through fuel cells or conventional combustion engines. Electrochemical upgrading, achieved via the electrochemical CO_2 reduction reaction (CO_2RR), could potentially produce a wide range of products, from carbon monoxide (CO) to hydrocarbons, under ambient conditions (Table 1).

In principle, any gas stream containing CO_2 can serve as the feedstock for CO_2RR, ranging from flue gas (~4–15% CO_2) to atmospheric air (~0.04% CO_2). In practice, however, the use of such dilute streams poses significant challenges (Figure 1A). Thermodynamically, the standard electrode potential required for CO_2RR shifts to more negative values as the concentration decreases, resulting in higher energy demand [11]. Kinetically, the reaction rate scales with CO_2 partial pressure, meaning that lower concentrations directly suppress the availability of CO_2 at the catalyst surface [12,13]. The presence of other gases further complicates selectivity. For example, oxygen (O_2) in flue gas or air can undergo two and four-electron transfer reduction in alkaline conditions [14]:

$$O_2 + H_2O + 2e^- \leftrightharpoons HO_2^- + OH^- \quad (1)$$

$$O_2 + 2H_2O + 4e^- \leftrightharpoons 4OH^- \quad (2)$$

In addition to affecting Faradaic efficiency through competing with CO_2RR, both routes lead to local alkalinity generation, that can convert CO_2 to HCO_3^- at the electrode surface and impede CO2RR. This formation of HCO_3^- might introduce additional complexities due to precipitation with present cations, further reducing Faradaic efficiency and device stability [15]. Other impurities such as nitrogen oxides (NOx) and sulfur oxides (SOx), present at trace levels in flue gas, can also lead to negative impacts. Thermodynamically, nitric oxide (NO), the most common NOx species, and sulfur dioxide (SO_2), the most common SOx species, exhibit more favorable reduction potentials than CO_2 (Figure 1B), and increase the risk of competing reactions. It is suggested that NOx impurities can reduce CO_2RR Faradaic efficiency due to their preferential reduction at the catalyst surface. Among different species, NO and NO_2 have shown to exert a stronger influence than N_2O because reduction of NO and NO_2 require more electron transfers than N_2O reduction [16]. Similarly, SO_2 have also introduced competing pathways, leading to a drop in CO_2RR Faradic efficiency [17]. Additionally, it is shown that SO2 can lead to irreversible damage on Cu catalyst and alter its selectivity toward formate, while it is a C_{2+}-designated catalyst [17].

View Article Online
DOI: 10.1039/D6EY00122J

From a process standpoint, using dilute CO_2 streams also necessitates energy-intensive separation of CO_2RR products from coexisting gases, particularly nitrogen (N_2) and O_2. Collectively, these thermodynamic, kinetic, selectivity, and process-level limitations strongly constrain direct CO_2RR from dilute sources, highlighting the need for a dedicated CO_2 separation step prior to electrochemical upgrading.

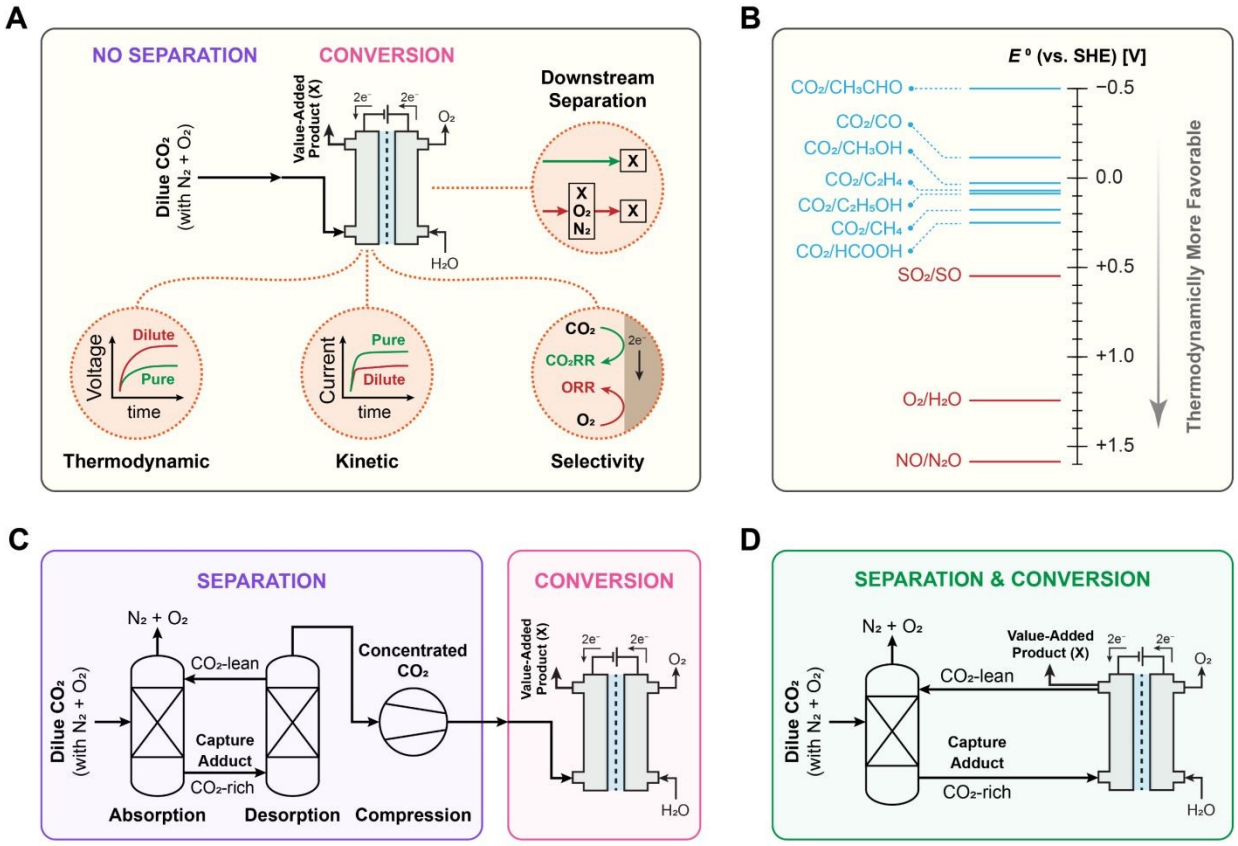

Figure 1. Challenges of CO_2RR from dilute streams and comparison of sequential and RCC routes. (A) In principle, any gas stream containing CO_2 can serve as the feedstock for CO_2RR to produce a desired product (X) without a prior separation step. In practice, however, the use of dilute streams poses significant challenges, including thermodynamic and kinetic disadvantages relative to pure CO_2 feeds, selectivity issues in producing the desired products, and the need for downstream separation from coexisting gases. (B) Standard reduction potentials of CO_2 to a range of products compared with O_2, NO, and SO_2, calculated under standard conditions at pH 0 using the Nernst equation. (C) Schematic of the sequential CO_2RR route, in which CO_2 is first separated from a dilute stream, and subsequently reduced in an electrolyzer (i.e., the conversion step). The separation step includes absorption and desorption to generate concentrated CO_2, which is subsequently compressed. (D) Schematic of the RCC route, in which separation and conversion are integrated: CO_2 absorbed from a dilute stream is directly supplied to the electrochemical conversion compartment without desorption and compression. In both routes, the oxygen evolution reaction (OER) from water is the most common anodic reaction.

CO_2 separation from dilute streams generally involves two steps: capture and concentration [18–20]. In the capture stage, CO_2 is selectively removed from the gas matrix using a sorbent (i.e., absorption), while in the concentration stage, the sorbent is regenerated, and the captured CO_2 is released (i.e., desorption). Amine scrubbing with thermal regeneration remains the most widely used approach, particularly for a wide range of flue gases [19]. However, these processes still

View Article Online
DOI: 10.1039/D6EY00122J

face persistent challenges, most notably the high energy requirements and sorbent degradation associated with the elevated temperatures required for regeneration [21,22]. Electrochemical alternatives are emerging as promising candidates to replace or complement thermal systems, offering advantages such as higher efficiency, modularity, scalability, and straightforward integration with existing infrastructure [23,24]. Importantly, they can operate under ambient conditions and rely solely on electricity as the energy input [25]. Electrochemical CO_2 separation can be broadly categorized into three mechanisms: electrochemical generation of nucleophiles (EGN) [26–29], pH-swing processes based on electrochemical modulation of proton concentration [30–37], and electrochemically mediated amine regeneration (EMAR) [21,22,38–41]. In each case, a cathodic reaction activates the sorbent to capture CO_2, while an anodic reaction regenerates the sorbent to release and concentrate CO_2. These processes have been demonstrated for separating CO_2 from a variety of dilute sources (e.g., flue gas, air, and more recently, seawater) and concentrating it into high-purity streams, which are subsequently compressed [41–43].

The compressed high-purity CO_2 generated from separation processes can be fed to CO_2RR systems, thereby eliminating the major challenges associated with using dilute streams. This route, where CO_2 is first captured, concentrated, and compressed before being supplied to the electrolyzer, is hereafter referred to as the *sequential process* (Figure 1C) [44]. Development of the sequential process, as the most common electrochemical approach for CO_2 upgrading, has attracted significant attention over the past few decades, leading to the demonstration of a wide range of gas-fed CO_2 electrolyzers [1,45,46]. Progress has been driven by advances in catalyst design, electrolyte formulation, membrane engineering, and reactor architectures, all of which have contributed to improved selectivity, current density, and energy efficiency [47,48]. The sequential process still remains an active area of research, with ongoing efforts focused on further enhancing performance and reducing cost to enable practical deployment [48–50].

Several steps in the sequential CO_2RR scheme impose relatively high energy demands and costs [19,51]. In particular, the concentration stage (i.e., CO_2 desorption and sorbent regeneration) and the subsequent compression of CO_2 are highly energy-intensive, together accounting for more than 70% of the total energy requirement of the separation process [52,53]. Moreover, fabricating and operating two independent systems (a separation unit and a CO_2RR electrolyzer) coupled with an intermediate compressor leads to elevated capital expenditures (CapEx) and operating expenditures (OpEx) [54,55]. An effective strategy to mitigate these challenges is to integrate separation and conversion into a single process. This can be achieved through electrochemical *reactive carbon capture* (RCC), in which CO_2 is first absorbed from a dilute stream (e.g. air, point sources) but, instead of being desorbed and compressed, is directly supplied to the electrochemical conversion compartment (Figure 1D) [56–61]. In this approach, CO_2 is electrochemically reduced in its captured state, theoretically eliminating both the energy-intensive desorption and compression steps [44]. RCC therefore offers the potential for lower CapEx (by requiring one integrated cell rather than two separate systems and avoiding compressors) and lower OpEx (by reducing electricity consumption associated with desorption and compression). Although RCC concepts have only recently emerged, early studies have demonstrated promising performance [57,60,62]. Still, RCC remains less mature and less understood compared to sequential CO_2RR, and progress requires a deeper understanding of thermodynamics,

View Article Online
DOI: 10.1039/D6EY00122J

electrochemical kinetics, catalyst and electrolyte interactions, membrane transport, and reactor configuration to enable scalable, low-energy CO_2 upgrading [56,63,64].

This Perspective provides a comprehensive assessment of electrochemical RCC by integrating advances in fundamental understanding, system development, and process and economic assessments into a unified framework. The work aims to contextualize RCC within the broader CO_2 conversion landscape and to establish a balanced, quantitative comparison with the conventional sequential processes. To achieve this, over one hundred studies were analyzed, the details of which are compiled in the *Supplementary Information*, covering both fundamental insights and benchmarking data. We began by revisiting the fundamental principles of CO_2RR and the sequential route, followed by analyzing potential energy savings in RCC and its unique mechanistic complexities. We then benchmarked the performance of RCC against sequential CO_2RR across several metrics, including current density, Faradaic efficiency, voltage, and energy intensity, and proceeded to examine techno-economic implications through operating and capital cost analyses. Lastly, we identified the most critical gaps that must be addressed for RCC to advance toward practical implementation, including system-level integration, catalyst design, microenvironment engineering, and stability.

What distinguishes this work from previous reviews is its holistic and updated approach. Earlier analyses of RCC have focused narrowly on electrochemical performance or reactor configuration, often in isolation from capture chemistry and process economics [65–69]. Here, by contrast, the capture–conversion interface is treated as a coupled system in which performance, energetics, and cost are inseparable. Moreover, this Perspective integrates the most recent breakthroughs published in 2025 and 2026 [70–76]—studies that have reshaped both the performance metrics and mechanistic understanding of RCC—allowing a reassessment of its true potential relative to sequential CO_2RR. This broader integration of scales, from molecular mechanisms to techno-economic feasibility, establishes a more balanced and realistic picture of RCC.

2. THE PRINCIPLES OF CO_2RR & THE CONVENTIONAL SEQUENTIAL ROUTE

The production of value-added chemicals by CO_2RR, both gaseous and liquid products, has been investigated using a variety of electrode (catalyst) configurations, electrolyte, and cell geometry; the details for which can be found in several review articles [48,77–79]. Briefly, CO_2 reduction occurs at the cathode, forming the product, and often O_2 is generated at the anode through the oxygen evolution reaction (OER). Simultaneous hydrogen evolution reaction (HER) has been consistently reported as the main parasitic reaction [4,80–82] while producing chemicals of interest by CO_2RR (Table 1). An electrochemical cell developed to produce CO, including a cathode and anode chambers, a separator, and gas diffusion electrodes (consisting of a current collector, a gas diffusion medium, and a metal catalyst layer), is demonstrated in Figure 2A-C. For the overall reaction, the Gibbs free energy (ΔG), which represents the thermodynamic minimum energy penalty to produce each product, can be estimated by considering both the number of electron transfers (n) and the standard reduction potential (E^0), i.e., $\Delta G = -nFE^0$, where F is the Faraday constant. The calculated ΔG values vary considerably across different CO_2RR products. In general, CO and formic acid (HCOOH) exhibit the lowest minimum energy penalties,

View Article Online
DOI: 10.1039/D6EY00122J

indicating that these products are thermodynamically more favorable to produce compared with hydrocarbons and multicarbon products (Figure 2D).

Table 1. Cathodic and Anodic Reactions in Electrochemical CO_2RR

Compartment	Path	Product	Reaction	$E°$ (V vs. SHE)*	Product Phase
Cathode	HER	Hydrogen	$2H^+ + 2e^- \rightarrow H_2$	0	Gas
	CO_2RR	Carbon monoxide	$CO_2 + 2H^+ + 2e^- \rightarrow CO + H_2O$	−0.106	Gas
		Formic acid	$CO_2 + 2H^+ + 2e^- \rightarrow HCOOH$	0.250	Liquid
		Methanol	$CO_2 + 6H^+ + 6e^- \rightarrow CH_3OH + H_2O$	0.016	Liquid
		Methane	$CO_2 + 8H^+ + 8e^- \rightarrow CH_4 + 2H_2O$	0.169	Gas
		Acetaldehyde	$2CO_2 + 10H^+ + 10e^- \rightarrow CH_3CHO + 3H_2O$	−0.5	Liquid
		Ethanol	$2CO_2 + 12H^+ + 12e^- \rightarrow C_2H_5OH + 3H_2O$	0.084	Liquid
		Ethylene	$2CO_2 + 12H^+ + 12e^- \rightarrow C_2H_4 + 4H_2O$	0.064	Gas
Anode	OER	Oxygen	$2H_2O \rightarrow O_2 + 4H^+ + 4e^-$	1.23	Gas

* *The values are adopted from the reference* [4,83]. *SHE stands for the standard hydrogen electrode.*

Over the past two decades, substantial progress has been made in tailoring catalysts to direct CO_2RR toward desired products. In this regard, CO_2RR literature has established a well-defined framework of descriptors that govern product selectivity, particularly the adsorption energies (ΔE) of key intermediates such as *CO and *H (ΔE_{*CO} and ΔE_{*H}) [82,84]. These parameters determine whether a catalyst surface favors CO_2RR over HER and which product pathway is preferred. As illustrated in Figure 2E, different catalyst families exhibit distinct product selectivities. Metals that bind *CO weakly, such as silver (Ag), gold (Au), and zinc (Zn) favor CO generation [82,85], whereas metals that bind *CO moderately but not *H, including indium (In), tin (Sn), mercury (Hg), thallium (Tl), and lead (Pb), predominantly yield HCOOH [82,85]. Other transition metals with strong *CO binding, such as nickel (Ni), palladium (Pd), and platinum (Pt), are less selective for CO_2RR and instead drive the HER, producing H_2 as the dominant product [82,85]. Copper (Cu), which binds *CO and *H with moderate and weak strength, respectively, uniquely enables the formation of hydrocarbons and multicarbon products, making it central to efforts on C_{2+} production [86–88].

View Article Online
DOI: 10.1039/D6EY00122J

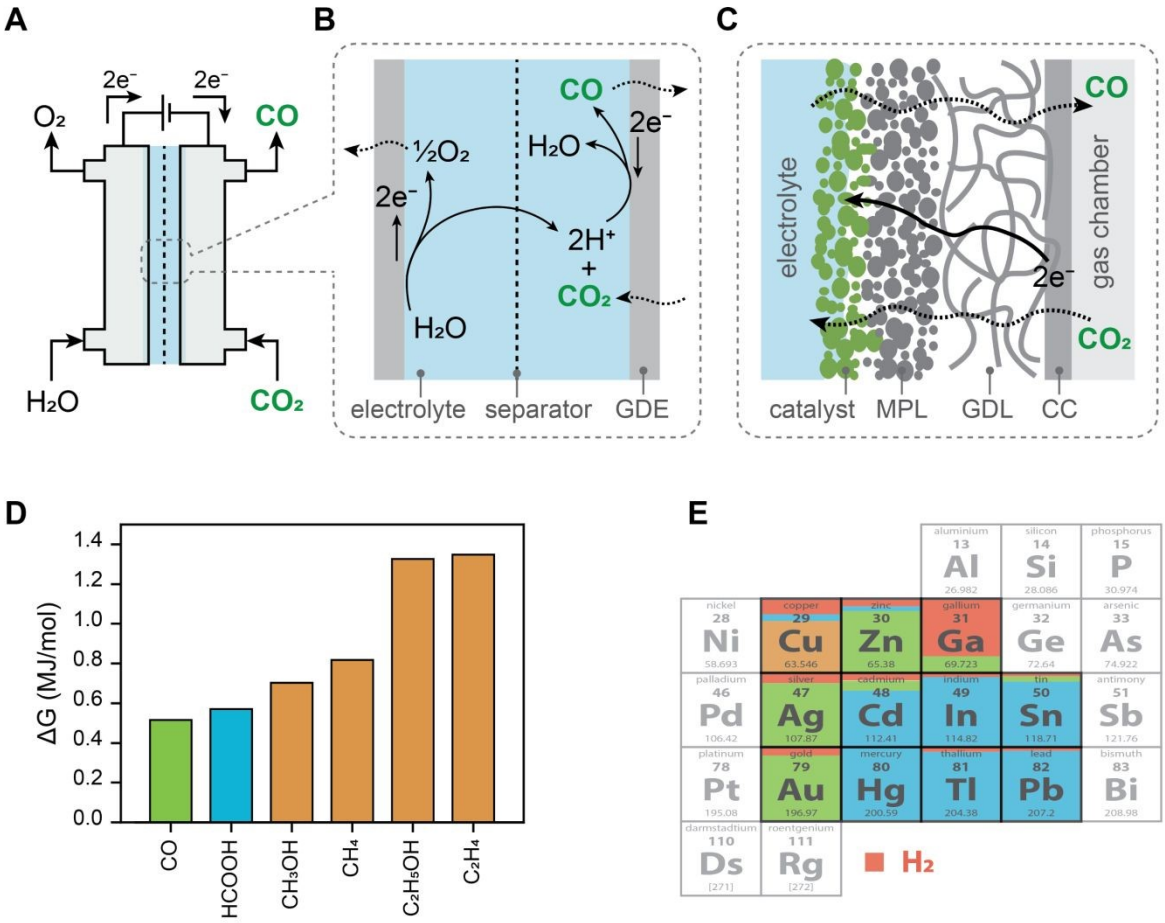

Figure 2. CO_2RR to produce a wide range of products. (A, B) Illustration of a representative electrochemical cell for CO production, consisting of cathode and anode chambers with gas diffusion electrodes (GDEs) separated by a separator. CO_2RR occurs at the cathode, while the OER takes place at the anode. (C) The GDE inserted between the gas chamber and the electrolyte generally includes a current collector (CC), a gas diffusion medium consisting of a gas diffusion layer (GDL) and a microporous layer (MPL), and a metal catalyst layer. The dashed arrows indicate the diffusion of the gaseous reactant (CO_2) and products (CO, O_2) through the GDE. (D) The Gibbs free energy of the electrochemical reaction has been estimated by considering the number of electron transfers and the standard reduction potential. (E) Chemical production through CO_2RR can be obtained by a variety of metal catalysts. The color and portion represent the product and corresponding selectivity, respectively.

The sequential systems operate on high-purity CO_2 in the gas phase as feed, supplied from an upstream separation process. This configuration represents the conventional route historically pursued for CO_2 electroreduction. Early studies relied on aqueous H-cell configurations with planar metal electrodes immersed in liquid electrolytes, where CO_2 was continuously bubbled through the solution [89]. However, the low solubility of CO_2 in aqueous media imposed severe mass transport limitations and restricted achievable current densities [89]. Modern gas-fed electrolyzers have overcome these constraints by employing GDEs to deliver CO_2 directly to the catalyst layer at the cathode, as implemented in flow cells and membrane electrode assemblies (as illustrated in Figure 1C). This architecture provides high surface area, short diffusion pathways, and rapid CO_2 transport within porous structures, enabling high Faradaic efficiencies

View Article Online
DOI: 10.1039/D6EY00122J

and current densities exceeding 1,000 mA/cm^2 [47,90]. Detailed descriptions of these reactor designs, their operation principles, and performance benchmarks have been comprehensively reviewed elsewhere [4,77,48,91,2].

These developments have advanced sequential CO_2 electrolyzers toward practical demonstrations, with state-of-the-art systems employing high-surface-area GDE catalysts and zero-gap configurations to enhance current density and reduce energy consumption [48,79,90]. The relatively high technology readiness levels (TRLs) achieved by these systems have enabled pilot-scale validation. For example, the Siemens/Evonik Rheticus project is operating a 25 kW stack of ten 300 cm^2 cells with anion exchange membranes (AEMs) for CO_2-to-syngas conversion, corresponding to TRL 5–6 [92,93]. Similarly, OCOchem company has commissioned a four-cell pilot, each with 15,000 cm^2 of GDE surface area, producing approximately 60 tons per year of formate ($HCOO^-$) under ambient conditions [94]. Additional commercial efforts (e.g., Dioxide Materials, Twelve/Opus12, Mantra) have demonstrated steady improvements in performance metrics such as current density and product selectivity. Despite these advances, several challenges continue to hinder large-scale deployment. First, unreacted CO_2 remains in the electrolyzer outlet stream, necessitating energy- and cost-intensive downstream separation from products. More critically, these systems depend on high-purity CO_2 as the feedstock, which is not readily available and must be supplied from an upstream separation process, adding both cost and logistical and technical complexity as discussed earlier.

3. CO_2RR VIA THE EMERGING RCC ROUTE

RCC is emerging as an alternative to the conventional sequential CO_2RR route, primarily motivated by the goal of lowering the overall energy demand and cost of the process. In the sequential processes, sorbent regeneration, CO_2 release, and compression account for most of the energy demand, while RCC aims to avoid these steps. Even though RCC in theory eliminates several energy-intensive steps of sequential processes, most of the developed RCC systems have demonstrated weaker performance metrics in terms of cell voltage, current density, and Faradaic efficiency, and consequently higher energy consumptions compared to those of sequential electrolyzers (as discussed later in Section 5). This is due to the more complex mechanistic landscape of RCC, which includes dynamic equilibria between dissolved CO_2, HCO_3^-, CO_3^{2-}, and carbamate species, governed by factors such as pH, CO_2 loading, catalyst, and the chemical nature of the capture media. This leads to transport limits and thus undesired reactions, introducing tradeoffs that hinder the improvement of all performance metrics simultaneously. Unlike sequential CO_2RR literature, which has plenty of fundamental studies [86,95,96], few studies have analyzed the reaction pathways and transport phenomena in RCC. In this regard, the sources of CO_2 and protons as the two main reactants for CO_2RR in RCC systems need to be carefully studied. In this section, two key areas are discussed to provide a better understanding of RCC potentials and challenges: the magnitude of potential energy savings achieved by RCC and the mechanistic complexities and tradeoffs with a focus on carbon and proton sources, reaction, and transport pathways.

View Article Online
DOI: 10.1039/D6EY00122J

3.1. Energetic Analysis

RCC energetics can be compared with the sequential route qualitatively (Figure 3A) and quantitatively (Figure 3B). Qualitatively, RCC lowers the minimum work by shifting the electrolysis reference state from concentrated CO_2 to the capture adduct, thereby bypassing the desorption and compression step of the sequential route. In Gibbs free-energy terms, the sequential route traverses two rises (i.e., capture to concentrated CO_2 and concentrated CO_2 to conversion intermediate/product), whereas RCC follows a single ascent from the capture adduct to the conversion intermediate/product. The inset in Figure 3A summarizes this reduction in the overall Gibbs free-energy span, indicating a potential thermodynamic advantage for RCC.

To quantitatively evaluate the potential reduction in energetics via RCC, a comparative model was developed [44]. The study examined a sequential and an RCC process designed to produce CO, each using a monoethanolamine (MEA)-based absorber followed by either a desorber together with a subsequent electrolyzer (i.e., sequential route) or an integrated electrolyzer (i.e., RCC route). The sequential route considers CO_2 electrolysis using state-of-the-art sequential systems with either 50% or 100% CO_2 single-pass utilization efficiency, reflecting *baseline* and *optimistic* possibilities. For RCC, three performance scenarios were considered: (i) an *optimistic* case (3 V, 90% Faradaic efficiency, and 50% single-pass utilization efficiency), (ii) a *baseline* case (4 V; 90% Faradaic efficiency; 30% single-pass utilization efficiency), and (iii) a *pessimistic* case (5 V; 70% Faradaic efficiency; 20% single-pass utilization efficiency) (Figure 3B). Under the optimistic case, the RCC route achieves a specific energy of 643 kJ/molCO_2, approximately 44% lower than the sequential benchmark. Under baseline conditions, the advantage diminishes and energy consumption approaches that of the sequential route (1,103 kJ/molCO_2). In the pessimistic case, integration becomes unfavorable, with energy consumption exceeding 2,400 kJ/molCO_2. These quantitative results suggest a clear design rule: integration is beneficial only when the RCC electrolyzer matches or surpasses the performance (such as cell voltage, Faradaic efficiency, and single-pass utilization efficiency) of the best sequential electrolyzers. Moreover, if future sequential electrolyzers achieve complete 100% CO_2 single-pass utilization efficiency, the maximum energy saving achievable via integration would decline to approximately 26%. This analysis was limited to CO production, and similar evaluations are still needed for other CO_2RR products to generalize these findings.

Despite the quantitative analysis that helped to have a better understanding of the magnitude of RCC energy savings for the first time, this analysis has several limits that necessitates further work. Firstly, this study was limited to CO production, and similar evaluations are still needed for other CO_2RR products to generalize these findings. Secondly, major parameters in this study were related to the CO_2RR and downstream separation steps, including Faradaic efficiency, cell voltage, and single pass conversion ratio. While these two steps are critical, more complex models that are sensitive to upstream CO2 capture parameters will be beneficial for better evaluation of energetics. This is particularly important as RCC systems have been proposed to capture CO_2 from various sources with different concentrations, such as air and flue gas, which have fundamental differences when it comes to energy demand. Overall, the observed energy savings are smaller than initially projected, primarily due to the lower performance metrics of current RCC systems relative to sequential ones. Nonetheless, because RCC inherently offers

View Article Online
DOI: 10.1039/D6EY00122J

potential for process integration and energy reduction, improving its electrochemical performance remains key to realizing its full energy-saving potential.

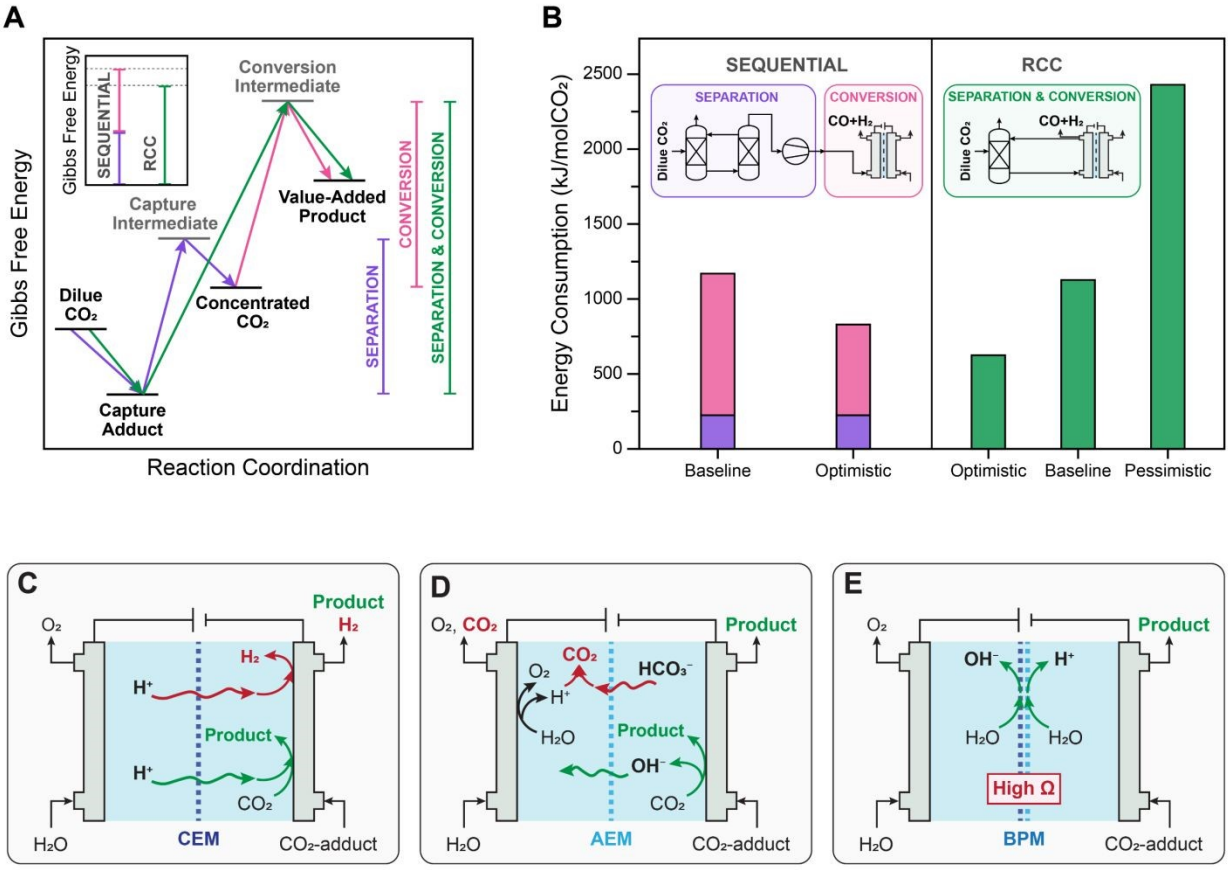

Figure 3. Energetic and configuration comparison between sequential and RCC routes. (A) Qualitative comparison of Gibbs free energy profiles for sequential and RCC routes, illustrating the additional desorption and compression step in the sequential route and the reduced overall free-energy span in RCC (inset). (B) Quantitative comparison of energy consumption between sequential and RCC routes, reproduced from ref. 44 with permission from nature portfolio [44], copyright 2022. In sequential, the separation energy (purple) includes amine regeneration and CO_2 compression, while the conversion energy (pink) accounts for CO_2 electrolysis, (bi)carbonate regeneration, and product separation. The sequential route reflects a state-of-the-art electrolyzer evaluated at either 50% or 100% CO_2 single-pass utilization efficiency, representing baseline and optimistic scenarios, respectively. For the RCC pathway, the total energy (green) associated with separation and conversion is provided, and three scenarios are considered: optimistic (3 V, 90% Faradaic efficiency, and 50% single-pass utilization efficiency), baseline (4 V; 90% Faradaic efficiency; 30% single-pass utilization efficiency), and pessimistic (5 V; 70% Faradaic efficiency; 20% single-pass utilization efficiency). (C–E) Schematic comparison of membrane configurations. (C) Cation exchange membrane (CEM) facilitates H^+ migration from the anode to the cathode, sustaining CO_2RR but promoting HER. (D) Anion exchange membrane (AEM) supports hydroxide (OH^-) transport toward the anode, favoring OER but allowing (bi)carbonate crossover and CO_2 release on the anode side. (E) Bipolar membrane (BPM) generates H^+ and OH^- via water dissociation to supply protons while minimizing (bi)carbonate crossover, though at the expense of higher ohmic (Ω) resistance and cell voltage.

View Article Online
DOI: 10.1039/D6EY00122J

3.2. Mechanistic Insights

The form of carbon (free dissolved CO_2 vs. bound adducts such as carbamates and (bi)carbonates) and the proton source impact reaction rates and pathways [61,63]. Three different scenarios are typically considered for the carbon source in RCC. Firstly, a *direct* route in which the bound adduct (e.g., carbamate or (bi)carbonate) is reduced without prior CO_2 release [56,61,64,97,98]. Secondly, a more common *indirect* route in which the captured CO_2 is first released as in-situ CO_2 (noted as "*i*-CO_2") and then reduced at the surface of the cathode [59,99–101]. A third hybrid pathway may also be possible, in which both routes occur [98]. These routes differ in thermodynamics and kinetics: direct reduction can avoid the desorption energy but requires activating a more complex, often anionic species. CO_2 adducts may be electronically pre-activated as a result of bent/partially charged structure (i.e., sp^2 hybridization with trigonal planar geometry) relative to linear CO_2 molecules (O=C=O), which can lower some barriers [58,65], yet the bulky CO_2-adduct and the negative charge of carbamate/(bi)carbonate oppose electromigration in the electrochemical double layer (EDL) and can hinder activation [60]. As for carbamate-mediated systems, e.g., when primary or secondary amines are used as the sorbent, some studies reported that CO_2 reduction proceeds primarily via *i*-CO_2 after carbamate dissociation, most likely due to the EDL formed by the large, ammonium cations (e.g., $R{-}NH_3^+$) that keep carbamates away from the cathode surface [60]. For instance, two studies have suggested that the primary pathway was through the reduction of *i*-CO_2 in solution, meaning that carbamate must first release *i*-CO_2 [97,100]. This has been confirmed by in-situ FTIR spectroscopy measurements as well [98]. However, in some specific cases, such as under sufficiently negative overpotentials [56], and complete removal of *i*-CO_2 by N_2 purging, direct carbamate reduction has been observed [60].

CO_2RR mechanistic landscape for (bi)carbonate-based systems, in which alkaline media such as KOH, K_2CO_3, and tertiary and sterically hindered amines are used as the absorbent, involves equilibria between *i*-CO_2 and (bi)carbonate species. At neutral to alkaline pH, most CO_2 in solution exists as HCO_3^- or CO_3^{2-} rather than CO_2 [102]. While computational work has suggested that the free energy barrier for the first electron transfer to HCO_3^- is on the same order as that for CO_2, meaning that, in theory, HCO_3^- could directly participate in CO_2RR [103], experimentally sustaining high reaction rates from HCO_3^- feeds often requires regenerating *i*-CO_2 [104]. Otherwise, a stagnant (bi)carbonate solution tends to generate a CO_2-starved cathode surface, and the overall rate drops as the system becomes limited by the (bi)carbonate to *i*-CO_2 conversion step [70,105].

In nonaqueous media, mechanistic insights are comparatively less developed. It has been suggested that CO_2RR in non-aqueous media proceeds through *i*-CO_2, similar to aqueous media [106]. Organic solvents generally have higher CO_2 solubilities than aqueous systems, which could potentially be advantageous; However, in aprotic media, protons needed for CO_2RR may come from slow, parasitic consumption of the solvent itself [58].

In addition to the capture media, catalyst material can also shift the reaction pathways. In a recent study, electrode-dependent mechanisms were investigated for MEA (a primary amine) and 2-amino-2-methyl-1-propanol (AMP; a sterically hindered amine) on Cu and Pb catalysts [61]. On the Cu electrode, the ammonium cations (in this case, either MEA-H^+ or AMP-H^+) could potentially

View Article Online
DOI: 10.1039/D6EY00122J

block the surface and hinder CO_2 reduction. MEA-H^+ prevents surface interaction with *i*-CO_2 due to strong surface binding and organized blockage, while AMP-H^+ allows limited CO_2 access due to its steric hindrance, which results in a weaker surface binding and subsequent blockage. In contrast, Pb showed enhanced CO_2 reduction performance with both amines, as weaker surface interactions in Pb create less passivation, resulting in more CO_2 access for the reduction reaction. These findings suggest that selecting capture media and catalyst materials needs to be strategically done to enhance the performance of CO_2RR in RCCs.

Regardless of the direct or indirect pathway for the reduction of CO_2, the capture media include several inherent trade-offs, which can be optimized to eventually improve the scalability of RCC. The first trade-off is related to the Lewis basicity of the capture medium and CO_2 speciation. Strong Lewis bases and CO_2-binding sorbents, such as primary amines and high-pH solutions (e.g., KOH), enhance capture efficiency and allow for smaller absorber units but stabilize CO_2 in less-reactive forms such as carbamates and carbonates. This stabilization increases the required overpotential and suppresses current densities during CO_2RR. In contrast, weaker-binding media such as tertiary or sterically hindered amines and moderate-pH solutions (e.g., K_2CO_3) facilitate CO_2RR at lower overpotentials but present disadvantages for the capture step by offering lower equilibrium capacity and slower uptake kinetics, thereby increasing the required absorber surface area [58,63]. For instance, in a direct air capture (DAC) scenario, CO_2 capture by KOH at pH ~14 to form K_2CO_3 at pH ~12 is feasible, but further conversion to $KHCO_3$ at pH ~8 would demand up to 14 times more air contactors and significantly higher fan energy due to the slower CO_2 absorption at lower pH [57,70,107].

The second tradeoff is related to the Lewis basicity of the capture medium and HER selectivity. Strong basicity or high pH in the capture media is advantageous for the capture step and suppressing HER at the cathode surface, but limits *i*-CO_2 and proton availability for CO_2RR [63]. Adjusting pH closer to neutral by tuning the capture medium, changing the CO_2 loading, or improving the proton supply through the membrane tends to facilitate CO_2RR but also introduces the risk of HER [61]. Therefore, a low pH supports *i*-CO_2 release, while a high pH promotes CO_2RR over HER [105,105,108]. This tradeoff becomes more pronounced at elevated current densities, where Faradaic efficiency drops sharply above ~100 mA/cm^2 as the catalyst becomes depleted of *i*-CO_2. [70]. Therefore, proton sources with intermediate strength are preferred: water or weakly acidic functional groups can facilitate the necessary protons for CO_2RR without completely directing selectivity towards HER. Methanol, being less acidic than water, suppresses HER [64]; however, it also makes protonation of CO_2 adducts more difficult, requiring higher overpotentials for reduction.

Cell configuration and membrane selection strongly influence local pH and ion distribution, which in turn impact Faradaic efficiency. Cation exchange membranes (CEMs) can facilitate proton migration from the anode to the cathode, but this requires a lower anolyte pH, which complicates OER at the anode and further promotes HER at the cathode (Figure 3C). Anion exchange membranes (AEMs) could be used to facilitate hydroxide transport towards the anode, which thermodynamically favors both cathodic CO_2RR and anodic OER reactions. However, they require alkaline conditions in the catholyte, complicating *i*-CO_2 and proton availability for CO_2RR on the cathode [109]. More importantly, AEM-based configurations suffer from (bi)carbonate crossover and migration toward the anode, where they release CO_2 at the anode, complicating

View Article Online
DOI: 10.1039/D6EY00122J

the process and requiring further CO_2 separation (Figure 3D). To eliminate the challenges of CEM and AEM, using a bipolar membrane (BPM)-based configuration has been explored to supply protons for the cathode while mitigating (bi)carbonate crossover by restricting anion migration (Figure 3E). Although BPMs assist by facilitating the crossover of desired ions and suppressing the crossover of unwanted species, they also introduce additional ohmic resistance and overpotential due to water dissociation, thereby increasing cell voltage and overall energy consumption [62,109–111].

4. RCC SYSTEM BENCHMARKING

There are several performance metrics that could be used in benchmarking the RCC systems. Current density, Faradaic efficiency, cell voltage, cathodic potential, CO_2 utilization efficiency, levelized energy consumption, power density, and energy efficiency are key performance metrics. Because most RCC reports emphasized current density and Faradaic efficiency and only a few provide additional metrics, here we opt to use partial current density (Faradaic efficiency multiplied by current density), cell voltage, and power consumption to represent product generation rate and energy intensity. In some RCC studies, the reported operating potential corresponds to the overall cell voltage, while in others only the cathode potential is provided (particularly for emerging capture media). To enable consistent benchmarking, both parameters were compiled, with all data adopted from the studies discussed in Supporting Information. Figure 4A shows partial current density as a function of cell voltage, whereas Figure 4B presents partial current density as a function of cathode potential. In each case, representative sequential studies reported in the same manner are included to allow direct comparison.

RCC systems generally exhibit significantly lower partial current densities than their sequential counterparts. For example, while sequential systems have achieved CO partial current densities exceeding 1,000 mA/cm^2, RCC systems that target CO plateau at around 200 mA/cm^2 (Figure 4), which is the result of a Faradaic efficiency drop in higher current densities. This disparity arises from multiple microenvironment constraints in RCC: (i) the availability of *i*-CO_2 near the catalyst interface is transport-limited due to the distance it needs to travel from the bulk to catalyst interface, after being released from carbamate or (bi)carbonate adducts; (ii) the negatively charged nature and bulky size of these bound species could hinder their migration across EDL, suppressing direct reduction of adducts; and (iii) competitive equilibria among *i*-CO_2, HCO_3^-, CO_3^{2-}, and carbamate species create additional transport and kinetic bottlenecks that are typically absent in sequential electrolyzers supplied with pure CO_2.

Comparing across capture media, RCC systems using (bi)carbonate solutions generally outperform those using carbamates, both in terms of partial current density and product diversity (Figure 4). (Bi)carbonate systems have generated CO, $HCOO^-$, CH_4, and C_{2+}, whereas carbamate systems have predominantly produced CO, with only a few demonstrations of other products such as acetate (CH_3COO^-). This difference reflects the weaker binding in (bi)carbonate relative to carbamate (C-O vs. C-N), which facilitates *i*-CO_2 generation that relies on proton flux from the membrane. By contrast, higher carbamate stability hinders *i*-CO_2 release, which is the result of much higher p*K*a of carbamates than that of (bi)carbonates [112]. This is essentially the

View Article Online
DOI: 10.1039/D6EY00122J

reason for the increasing temperature and pressure in most of the carbamate studies. The former can facilitate *i*-CO_2 release through C-N cleavage, and the latter can increase *i*-CO_2 concentration through controlling vapor-liquid equilibrium [63]. Emerging capture media, including DES and IL-based systems, currently deliver partial current densities one to two orders of magnitude lower than those achieved with carbamate and (bi)carbonate media or sequential systems. Nevertheless, their tunability has enabled the formation of unique products such as oxalate and succinate, and other C_{2+} products (Figure 4B), highlighting their potential to expand the product space even if present performance remains limited.

Power density can serve as a practical indicator of the energy demand of CO_2RR systems. It was estimated by multiplying the reported total current density by the corresponding cell voltage. Whereas partial current density reflects the rate of generation of a target product, total current density captures the overall electron flux that must be supplied, and thus directly determines the electrical energy input. Because cell voltage is required for this calculation, only RCC studies reporting full-cell voltages were included in the analysis. The results show that, on average, RCC systems exhibited lower power consumption compared with sequential CO_2RR (Figure 4C). While reducing power density is desirable for any electrolysis system, this should be achieved by increasing Faradaic efficiency—maximizing the desired reaction rate for a given total current—and by minimizing overpotential losses arising from catalyst activation or resistance in the electrolyte and membrane. In RCC, however, the lower observed power density compared to sequential systems does not reflect targeted voltage optimization; instead, it results primarily from the lower total current densities typically achieved in RCC cells.

Overall, these benchmarking results show that no single metric fully captures the performance of RCC compared with the sequential route. Sequential systems consistently achieve higher partial current densities due to their superior kinetics and transport properties, aided by optimized gas-fed electrolyzers and direct CO_2 availability, whereas RCC suffers from additional complexity associated with equilibria between *i*-CO_2 and bound adducts. Nevertheless, RCCs (in particular, (bi)carbonate media) have the potential to be improved with more *i*-CO_2 availability near the cathode interface, to increase Faradaic efficiency, and reduce cell voltage, most of which could be achieved by membrane (in particular, BPMs) optimization. The comparison between the two routes can also extend beyond electrochemical metrics to include capital and operating expenditures. These techno-economic aspects are considered in the next section.

View Article Online
DOI: 10.1039/D6EY00122J

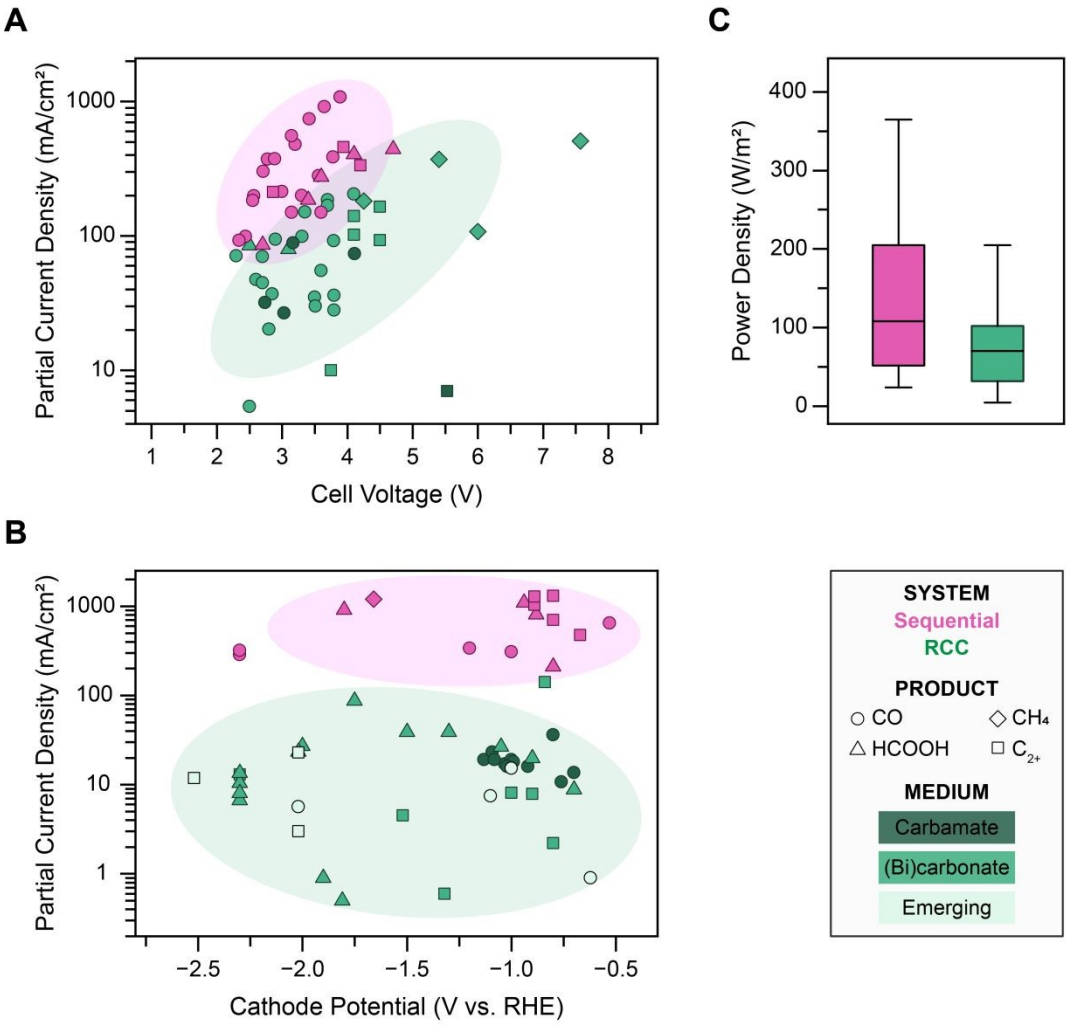

Figure 4. Benchmarking RCC and sequential CO_2RR performance. Partial current densities (mA/cm^2) of RCC systems are compared with sequential CO_2RR counterparts as a function of (A) cell voltage (V) and (B) cathode potential (V vs. reversible hydrogen electrode; RHE). (C) The corresponding power densities for RCC and sequential systems are presented. Partial current density was calculated as the product of total current density and Faradaic efficiency for a given product, while power density was obtained by multiplying total current density by the cell voltage. Three different capture media (carbamate, (bi)carbonate, and emerging media such as DES and IL) were considered to produce a wide range of products, including carbon monoxide (CO), formic acid (HCOOH), methane (CH_4), and multicarbons (C_{2+}) (e.g., ethylene, acetate, oxalate, and succinate). Data were compiled from recent studies across both systems, as discussed in Section 4 and the *Supplementary Information*.

5. ECONOMICS OF RCC

To fully assess the advantages of RCC compared with the sequential route, economic considerations must be evaluated alongside technical performance metrics. Techno-economic analysis (TEA) provides a systematic framework for this purpose, allowing CapEx and OpEx to be quantified and benchmarked against market conditions. TEA is therefore an essential tool for determining whether the reductions in energy demand and process complexity offered by RCC can translate into economic competitiveness compared to the sequential approach. Despite the availability of an extensive TEA literature for sequential processes, only a limited number of

View Article Online
DOI: 10.1039/D6EY00122J

studies have examined the economic feasibility of RCC systems [113–115]. Here, we compiled and further analyzed the outcomes of these RCC-focused TEAs to derive comparative insights on the production costs of CO_2-derived products relative to sequential routes. It is important to note that most of these studies are based on current RCC performance metrics, which reflect the lower TRL of RCC compared with sequential systems. Consequently, the economic trends and benchmarks discussed here may evolve as RCC systems mature and higher TRL demonstrations achieve improved performance metrics.

Due to the low TRL of RCC, most TEA studies have provided only high-level cost estimates without a detailed breakdown. Only one recent study reported both OpEx and CapEx distributions across different products [116]. In this study, the OpEx breakdown was provided for five products—two gaseous (CO and C_2H_4) and three liquid (HCOOH, CH_3OH, and C_2H_5OH)—while CapEx details were reported only for CO and HCOOH. As for OpEx, RCC processes generally showed comparable values to sequential processes for gaseous products but higher costs for liquid products (Figure 5A). The elevated OpEx for liquid products is primarily due to the additional cost of downstream separation. In RCC systems, liquid product concentrations are substantially lower than in sequential systems, which necessitates more energy-intensive separation steps. Among the conventional liquid ohase separation methods, liquid liquid extraction is not a relevant option due to significant complexities caused by the added solvent, and thermal distillation is costly and energy-intensive. In addition, unlike gaseous products that can in principle leave the electrolyzer in the gas phase, liquid products remain dissolved in the liquid capture medium that is intended to be recirculated for continued CO_2 absorption. As a result, these products do not only create a downstream separation challenge, but can also alter the composition of the recycled medium and potentially interfere with its reuse for CO_2 capture. For instance, in the case of organic acids, such as formic acid (pKa ~3.75) and acetic acid (pKa ~4.75), the alkalinity of medium will be consumed by the liquid product and severely reduce the available alkalinity for the CO_2 absorption step. Therefore, the presence of liquid products can impose an additional burden on maintaining stable operation and restoring the medium to a composition suitable for recycle. In the currently available TEA, these downstream costs are dominated by thermal distillation. Such separation requirements offset the savings achieved by eliminating upstream CO_2 processing in RCC. For C_2H_4, RCC exhibited slightly higher OpEx than sequential CO_2RR. This increase is attributed to higher power consumption, reflecting the current low TRL of RCC systems for C_2H_4 production. Specifically, higher overpotentials, lower current densities, and lower Faradaic efficiencies compared with more mature sequential electrolyzers contribute to this elevated energy demand. CapEx was reported only for CO and HCOOH. For both products, RCC showed higher capital costs compared to the sequential systems (Figure 5B). While the difference for CO was modest and within a comparable range, the CapEx for HCOOH was substantially higher, driven by the significantly larger downstream separation requirements dominated by distillation. In general, gaseous products are less costly to recover from the liquid electrolyte in RCC, whereas liquid products impose a considerably higher energy and cost penalty due to the need for separation from the liquid capture media.

Taken together, the OpEx and CapEx results indicate that the savings expected from RCC, primarily through the elimination of upstream CO_2 processing, are often offset by the high cost of downstream product separation if the electrolyzer performance metrics stay at current levels. As a result, the commonly perceived advantage of RCC in lowering both CapEx and OpEx is not necessarily realized at the current stage of development. This highlights the need for improvements in electrolyzer performance (e.g., current density, Faradaic efficiency, cell voltage)

View Article Online
DOI: 10.1039/D6EY00122J

for the gaseous products. However, this may not be enough to reduce CapEx and OpEx for liquid products due to the energy-intensive downstream distillation process, highlighting the need to redesign separation strategies with the explicit goal of replacing energy-intensive thermal distillation. Potential alternatives could be electrochemical separations [117,118] or membrane-based separations [119,120], which could reduce both energy demand and cost relative to conventional distillation.

We also analyzed the levelized cost of production (LCOP) reported in several studies for CO, HCOOH, and C_2H_4 for both sequential and RCC processes [1,54,55,113–116,121–126]. LCOP accounts for both OpEx and CapEx, normalized to the quantity of product generated. For reference, market prices of the products are also shown (Figure 5C). For gaseous products (CO and C_2H_4), the LCOP values of RCC were generally comparable to those of sequential processes, spanning similar ranges. For CO, the LCOP of sequential systems was reported at 0.40 ± 0.20 \$/kg, while RCC showed a slightly higher but overlapping range of 0.66 ± 0.29 \$/kg. For C_2H_4, the sequential route yielded an LCOP of 1.80 ± 1.23 \$/kg, compared to 1.25 ± 0.83 \$/kg for RCC. The variation in LCOP of RCC reflects variation in reported RCC performance metrics such as applied potential, current density, and Faradaic efficiency. In contrast, for the liquid product HCOOH, the reported LCOP value for RCC (\$7.42/kg) was substantially higher than the range reported for sequential systems (0.94 ± 0.77 \$/kg). This discrepancy arises from the high OpEx and CapEx contributions associated with downstream separation in RCC, as discussed earlier. It should be noted, however, that the RCC LCOP value for HCOOH is based on a single study; therefore, drawing firm conclusions at this stage is premature. Additional TEA efforts specifically targeting liquid products, particularly HCOOH, are needed to more definitively evaluate their economic feasibility in RCC systems.

To further assess cost competitiveness, the net revenue gap (NRG) was calculated as the difference between the LCOP and the market price for CO, HCOOH, and C_2H_4 (Figure 5D). For CO, both sequential and RCC routes yielded NRG values close to zero, with slightly positive margins, suggesting that CO production is approaching market viability. However, further improvements in performance metrics are required to enhance profitability and achieve consistently higher positive NRG values. For HCOOH, the RCC route exhibited a strongly negative NRG (−6.73 \$/kg), reflecting the high cost penalties associated with downstream liquid–liquid separation. This observation is based on a single detailed study, as discussed earlier, and additional TEA efforts targeting liquid products are needed to confirm the generality of this result. For C_2H_4, both sequential and RCC processes showed wide variability in NRG, with mostly negative values. RCC displayed a slightly less negative NRG on average, consistent with its somewhat lower LCOP compared to sequential systems.

Overall, these TEA results suggest that RCC is currently more favorable for gaseous products such as CO and C_2H_4, where it can achieve near-competitive costs relative to sequential processes. Nevertheless, significant advances in technical performance metrics (e.g., higher current density, Faradaic efficiency, and reduced cell voltage) will be required to further reduce costs and secure market competitiveness. For liquid products, the economic feasibility of RCC remains uncertain, and targeted research into alternative separation strategies will be essential to fully unlock its potential.

View Article Online
DOI: 10.1039/D6EY00122J

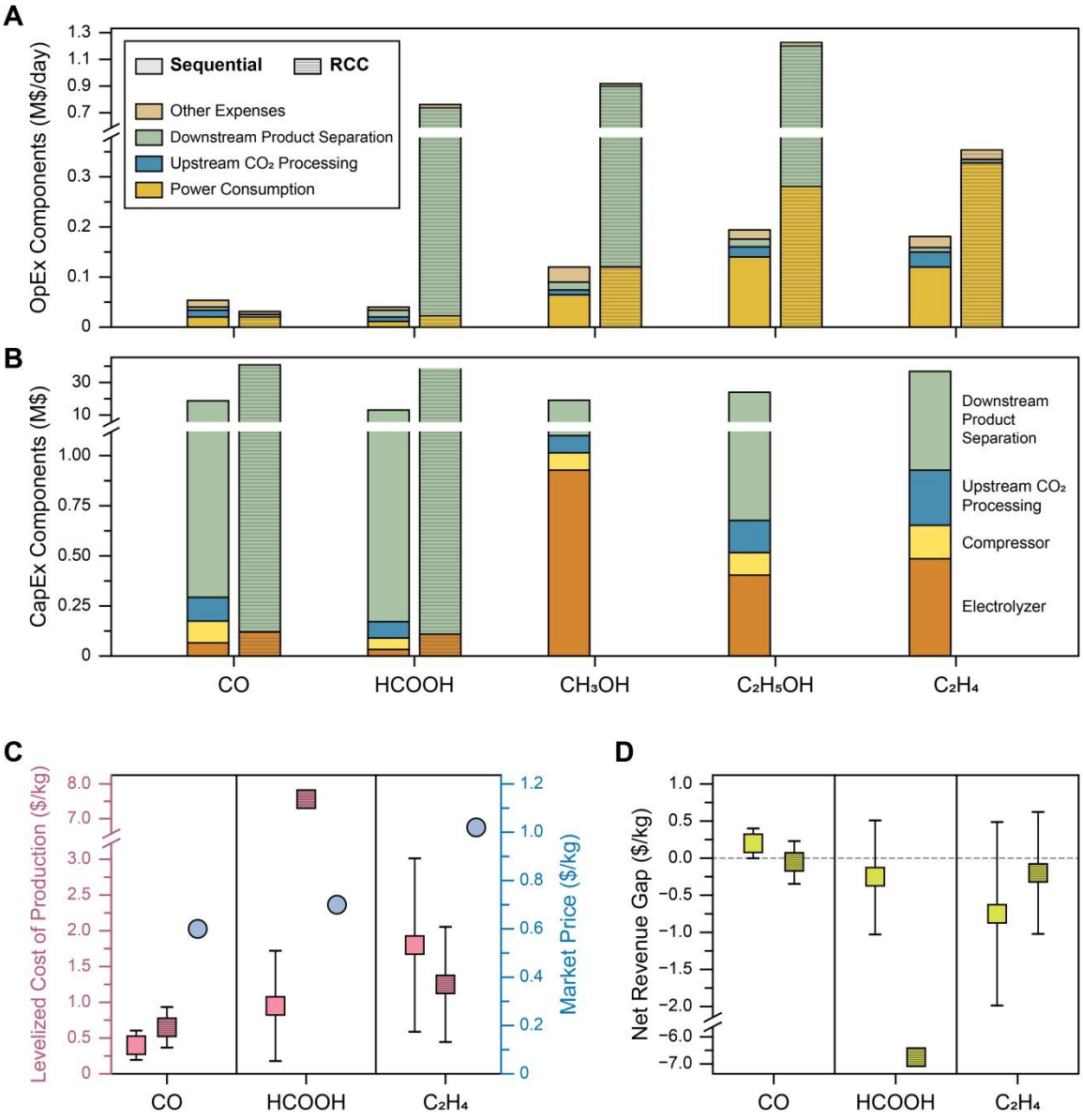

Figure 5. Techno-economic benchmarking of sequential and RCC processes. (A) Operational expenditure (OpEx) breakdown for carbon monoxide (CO), formic acid (HCOOH), methanol (CH_3OH), ethanol (C_2H_5OH), and ethylene (C_2H_4) via the sequential and RCC (patterned) routes. Power consumption corresponds to the electricity required for CO_2RR; upstream CO_2 processing refers to the capture stage required only for sequential systems; downstream product separation reflects the cost of separating products (liquid: HCOOH, CH_3OH, C_2H_5OH; gas: CO, C_2H_4) from the RCC electrolyte; and "Other Expenses" include feedstock, labor, maintenance, component replacement, and taxation/depreciation. Panel A was reproduced from ref. 116 with permission from RSC Publishing [116], copyright 2025. (B) Capital expenditure (CapEx) breakdown for sequential systems (all five products) and RCC (CO and HCOOH only). For sequential systems, costs include the electrolyzer, compressor, upstream CO_2 processing, and downstream product separator. For RCC, only the electrolyzer and downstream separator are required. For HCOOH in RCC, the downstream separation cost is substantially larger than the plotted range; the top of the bar is left open to indicate this without displaying a precise value, due to uncertainty in reported estimates. Core data for panels A and B were adopted from ref. [116], with cost components regrouped for clarity. (C) Levelized cost of production (LCOP) and market prices for CO, HCOOH, and C_2H_4, the only products with reported LCOP values. (D) Net revenue gap (NRG), calculated as the difference between LCOP and market price, for CO, HCOOH, and C_2H_4. In panels C and D, error bars represent standard deviations of values reported across multiple studies [1,54,55,113–116,121–126]. The

View Article Online
DOI: 10.1039/D6EY00122J

spread in RCC LCOP values reflects variations in reported performance metrics, including applied potential, current density, and Faradaic efficiency.

6. RCC: WHAT REMAINS TO BE EXPLORED

The preceding sections summarized *what has been achieved* in RCC, highlighting its potential energetic advantages relative to the sequential route, along with the associated limitations, tradeoffs, and techno-economic implications that identify gaseous products as the most promising near-term targets. Despite this progress, RCC research remains at an early stage, and several critical gaps must be addressed to match the performance metrics of sequential systems and enable higher TRLs. These gaps can be grouped into three domains. First, RCC studies have largely overlooked the system-level (i.e., holistic) perspective, with alkalinity regeneration often neglected while most efforts focus narrowly on CO_2RR metrics. Second, achieving high partial current densities remains challenging due to incomplete understanding and control of the electrochemical microenvironment and transport processes that span multiple length scales. Finally, long-term stability, both chemical and operational, has not been comprehensively studied, despite its importance for scaling and durability. This section focuses on *what remains to be explored*, elaborating on the critical gaps that must be addressed to advance RCC development toward practical implementation.

6.1. System-Level Integration and Alkalinity Regeneration

Most RCC studies have primarily focused on CO_2RR performance metrics, with only a few adopting a complete system-level perspective that includes both capture and conversion. In particular, the alkalinity regeneration—an equally critical step alongside CO_2RR—has been largely overlooked. In a typical RCC scheme (Figure 1), CO_2 is first absorbed from a dilute stream using a sorbent, followed by simultaneous CO_2RR and sorbent regeneration via alkalinity recovery, which enables continuous CO_2 separation in the absorber. To quantify this aspect, the electron–alkalinity (EA) efficiency can be used, defined as the ratio of OH^- (alkalinity) generated to the total electrons passed in the RCC electrolyzer [127]. This global metric highlights the degree to which RCC can sustain the absorber–electrolyzer cycle and is also applicable to related electrochemical carbon capture (ECC) systems.

The maximum theoretical EA efficiency depends on design parameters, including the dominant CO_2 carrier in the absorber (e.g., HCO_3^- vs. CO_3^{2-}), and the targeted CO_2RR product. To illustrate these dependencies, two simplified scenarios are considered: an ideal case with 100% EA efficiency (Figure 6A) and a practical case in which EA efficiency decreases below 100% (Figure 6B). In both scenarios, the passage of *n* moles of electrons through the cell drives the transport of *n* moles of H^+ across the membrane. Assuming the CO_2-rich absorber effluent is primarily HCO_3^-, these H^+ react with *n* moles of HCO_3^- to generate *n* moles of *i*-CO_2, which is then available for reduction at the cathode. In the ideal case, all *n* moles of *i*-CO_2 are consumed to form *n* moles of the desired product (C) and *n* moles of OH^-, yielding full recovery of alkalinity (Figure 6A). This results in an EA efficiency of 100%, as every electron contributes to both product formation and complete regeneration of the sorbent. In the practical case, however, there is a potential stoichiometric mismatch between the number of electrons transferred (*n*) and the number of

View Article Online
DOI: 10.1039/D6EY00122J

carbon units (*m*) that can be incorporated into the product. Only *m* moles of *i*-CO_2 are consumed to generate *m* moles of product and *m* moles of OH^-. The remaining (*n*−*m*) moles of *i*-CO_2 are reabsorbed in the cathode chamber as HCO_3^- by reaction with the corresponding OH^-, thereby reducing the net OH^- available for alkalinity regeneration to *m* rather than *n* (Figure 6B). This lowers the EA efficiency from 100% to *m*/*n* × 100%. As a result, the absorption capacity of the upstream capture stage is diminished, and (*n*−*m*) moles of CO_2 are expected to remain unabsorbed in the absorber effluent under hypothetical complete capture conditions.

These scenarios assume an idealized Faradaic efficiency of 100% for CO_2RR (FE_{CO2RR}), representing an upper bound that has not been experimentally realized. The impact of Faradaic efficiency on EA is linear, such that any inefficiency proportionally reduces EA according to: EA(%) = FE_{CO2RR} × (*m*/*n*) × 100. This occurs because, instead of producing *m* moles of C, only (FE_{CO2} × *m*) moles are formed, which consumes an equivalent amount of *i*-CO_2. The remaining unreacted *i*-CO_2 stays in the cathode solution, thereby proportionally lowering the amount of alkalinity regenerated by consuming OH^-. Thus, deviations from both stoichiometric and Faradaic ideality result in reducing EA efficiency.

To further illustrate the upper limits of EA efficiency, we evaluated an exemplary RCC system designed to produce CO from an HCO_3^- medium. At the anode, OER generates 2 moles of electrons (*n* = 2) and 2 moles of protons ($H_2O \rightarrow ½\ O_2 + 2H^+ + 2e^-$). These protons migrate through the membrane and react with 2 moles of HCO_3^- to form 2 moles of *i*-CO_2. At the cathode, the transfer of 2 electrons results stoichiometrically in the formation of 1 mole of CO (*m* = 1) and 2 moles of OH^-, while consuming 1 mole of *i*-CO_2 ($CO_2 + 2e^- + H_2O \rightarrow CO + 2OH^-$; equivalent to the reaction in Table 1 but rearranged to show OH^- explicitly). The remaining unconsumed 1 mole of *i*-CO_2 (i.e., *n*−*m*) is reabsorbed by 1 mole of OH^-, leaving a net generation of 1 mole of OH^-, from 2 moles of electron, to be recycled to the absorber instead of 2. As a result, the EA efficiency is reduced to 50% (i.e., 1/2 × 100). The same stoichiometric logic can be extended to other CO_2RR products by applying their respective electron-transfer (*n*) and carbon-incorporation (*m*) values, which determine the theoretical upper limits of EA efficiency for each case. The values of *n* and *m* for different CO_2RR products are summarized in Figure 6C.

If CO_2 is absorbed as CO_3^{2-} rather than HCO_3^-, the theoretical maximum EA efficiency for a given product doubles. This is because less *i*-CO_2 is generated per mole of H^+ transferred through the membrane: one mole of H^+ reacts with HCO_3^- to release one mole of CO_2, whereas the same proton flux reacts with CO_3^{2-} to generate only half a mole of CO_2. The maximum theoretical EA efficiencies for different products in HCO_3^- and CO_3^{2-} media are shown in Figure 6D. The decline in EA efficiency becomes more pronounced for products that require larger numbers of electron transfers (e.g., C_2H_5OH and C_2H_4). For instance, in HCO_3^- medium, the maximum EA efficiency decreases from 50% for CO (*n* = 2, *m* = 1) to 16.67% for C_2H_4 (*n* = 12, *m* = 2). As with HCO_3^-, Faradaic efficiency exerts a proportional effect in CO_3^{2-} media; in this case, the relationship is given as: EA(%) = FE_{CO2RR} × (2*m*/*n*) × 100.

While the theoretical EA efficiency is derived from stoichiometric ratios, and is therefore useful for identifying the upper bounds imposed by product type and capture medium, it does not account for thermodynamic, kinetic, or transport limitations that will further reduce EA efficiency in practical RCC operation. In real systems, the attainable EA efficiency is also governed by the Faradaic

View Article Online
DOI: 10.1039/D6EY00122J

efficiency toward CO2RR, because any loss in selectivity directly lowers the fraction of electrons that regenerate useful alkalinity. In carbonate-based systems, this relationship can be expressed as EA(%) = FE_{CO2RR} × (2m/n) × 100, showing that deviations from ideal CO2RR selectivity proportionally reduce EA efficiency. In RCC, such losses may arise from slow release of in situ CO_2 (*i*-CO_2) from captured species, limited transport of *i*-CO_2 to the catalyst surface, and mass-transport bottlenecks associated with bulky or charged CO_2 adducts and capture-derived ions within the electrochemical double layer. These constraints can lower the local availability of *i*-CO_2, increase competition from HER, and thereby diminish the practical EA efficiency below its stoichiometric limit. The formic acid pathway also requires additional consideration because product speciation depends on the pH of the medium. If the product remains in its deprotonated form as formate rather than protonated formic acid, the corresponding upper limit of EA efficiency decreases from 100% to 50%. Therefore, even among the stoichiometrically most favorable RCC products, the practically attainable EA efficiency remains sensitive not only to product identity, but also to selectivity, local reaction environment, and product speciation.

Given the inherent similarities between ECC and RCC systems—both of which aim to regenerate alkalinity through an electrochemical step to sustain the capture loop—the EA efficiencies of RCC can be benchmarked against those of ECC. For reference, ECCs based on EMAR have theoretical EA efficiencies of 50%, while ECCs employing EGN (e.g., quinone-based systems) have theoretical EA efficiencies of 100% [23,29,128,129]. Experimental studies further confirm that both approaches can maintain high EA efficiencies over extended operation times [22,29,39,40,130].

These theoretical limits highlight the critical role of product selection and capture medium in determining the practicality of RCC systems. To fully assess this viability, system-level analyses must also complement TEA results. While TEA indicated that gaseous products such as CO and C_2H_4 are more economically competitive than liquid products, those assessments did not account for EA efficiency as a defining system-level parameter of RCC. As shown by the theoretical analysis here, products such as C_2H_4 that require higher electron transfers inherently suffer from very low maximum EA efficiencies. From an economic standpoint, this translates into increased required surface area and make-up absorbent demand in the absorption step, leading to substantially higher CapEx and OpEx [107]. Taken together, both TEA and EA considerations point to CO as the most promising target product for RCC. Future studies must therefore prioritize improving Faradaic efficiency for CO in order to raise EA efficiency closer to its theoretical maximum. Strategies to enhance Faradaic efficiency will be further discussed in the next section.

View Article Online
DOI: 10.1039/D6EY00122J

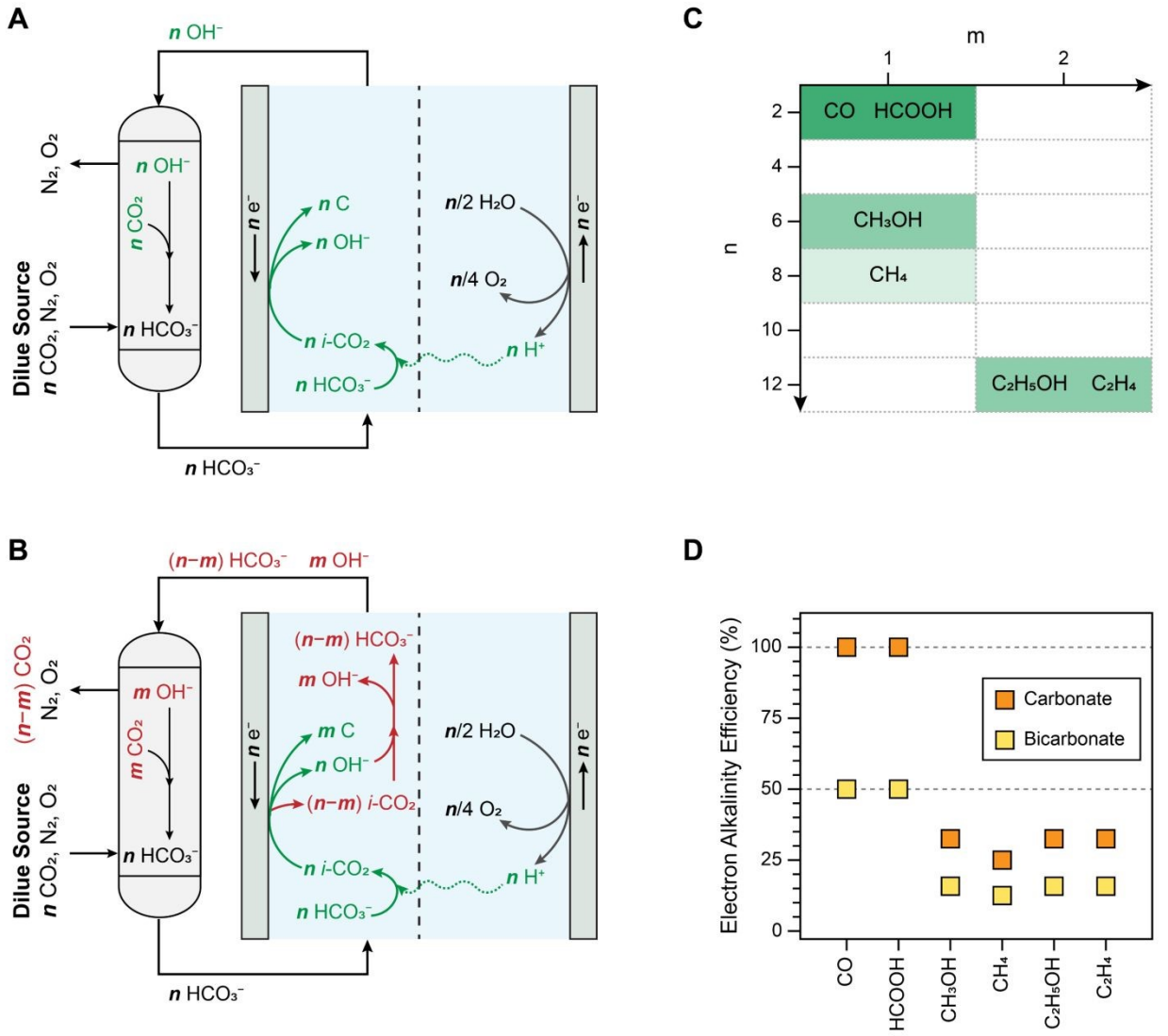

Figure 6. Theoretical limits of electron–alkalinity (EA) efficiency in RCC. (A) *Ideal scenario*. In an RCC system operating with bicarbonate (HCO_3^-) as the dominant CO_2 carrier, the passage of n electrons across the cell generates n protons at the anode (via OER), which react with n HCO_3^- to form n i-CO_2. At the cathode, all n i-CO_2 are reduced to form n carbon units in the desired product (C) and n OH^-, resulting in complete sorbent regeneration and an EA efficiency of 100%. (B) *Practical scenario*. In practice, a stoichiometric mismatch arises between the electrons transferred (n) and the carbon units incorporated into products (m). Therefore, only m moles of i-CO_2 are consumed to form m moles of product C and m OH^-, while the remaining (n−m) i-CO_2 recombines with OH^- to reform HCO_3^-. This reduces the net alkalinity generated to m OH^- instead of n, lowering EA efficiency to (m/n × 100%). The schematic illustrates this imbalance, where (n−m) CO_2 escapes with the absorber effluent. (C) Summary of electron requirements (n) and carbon incorporation numbers (m) for major CO_2RR products. Products requiring higher electron numbers (e.g., C_{2+} products) inherently yield lower theoretical EA efficiencies, represented by the intensity of the green color used. (D) Calculated maximum EA efficiencies for RCC in carbonate (orange) and bicarbonate (yellow) media across different products. For carbonate systems, efficiencies are doubled because fewer i-CO_2 molecules are generated per mole of H^+ transported. The results show a strong dependence of EA efficiency on product choice and capture medium. The two dashed lines serve as references, corresponding to EA efficiencies reported for ECC systems: 50% for EMAR and 100% for EGN.

View Article Online
DOI: 10.1039/D6EY00122J

6.2. Microenvironment Control to Enhance Partial Current Density

The lower partial current densities achieved in RCC systems than their sequential CO_2RR counterparts (as shown in Figure 4) highlight a key research gap in the limited understanding and control of the electrochemical microenvironment. In the sequential route, continuous CO_2 supply ensures CO_2 availability near the catalyst interface. In contrast, RCC relies on the transport of *i*-CO_2 from the bulk to the catalyst interface, where its limited availability has led to a drop in Faradaic efficiency at higher current densities and HER domination to allow for the demanding current densities. Furthermore, local alkalinity generated from both CO_2RR and HER recaptures *i*-CO_2 as HCO_3^-, leading to deactivation, which is referred to as *i*-CO_2 exhaustion by OH^- [131]. Consequently, within the higher ranges of achieved total current density in RCC (~100 – ~500 mA/cm^2), the overall CO_2RR rate (i.e., partial current density) is governed by *i*-CO_2 availability near the cathode interface rather than by the intrinsic catalytic activity of the electrode.

To address these limitations, several recent studies have focused on microenvironment engineering to improve mass transport and reaction kinetics [132,133]. Electrolyte modifications, including the addition of surfactants such as CTAB to suppress HER [134], or tuning background cations to modulate EDL thickness [60], have shown measurable improvements in Faradaic efficiency in modest current densities up to 100 mA/cm^2. To further increase partial current density, several strategies beyond electrolyte optimization, focused on electrode local architecture at different scales, have been employed to enhance *i*-CO_2 activity at the interface. These strategies include the incorporation of additional coating or tuning the catalyst support's porosity at different scales. The first strategy was based on redox-active polymeric frameworks with viologen branches that can undergo reduction and directly bind *i*-CO_2 and activate it. This coating layer was suggested to act as a mediator between the catalyst and *i*-CO_2, which can bind and pre-activate *i*-CO_2 as $*CO_2$ intermediates, facilitating its subsequent reduction [131]. This strategy led to achieving a C_{2+} Faradaic efficiency of 55 ± 5% at 300 mA/cm^2. Secondly, hierarchical catalyst support with multi-scale pores, instead of planar and nano-porous supports, was employed [70]. Planar catalyst supports suffer from limited catalytically active sites for interaction with *i*-CO_2. Using supports with nanoscale pores (<2 nm) could improve the active area due to the high porosity, but the tight area can hinder *i*-CO_2 diffusion and intensify the *i*-CO_2 exhaustion effect. A more effective architecture suggested in this study was using a two-scale carbon scaffold in which larger pores (~2–50 nm) provide fast transport channels that supply *i*-CO_2 for a secondary network of pores (<2 nm), combining abundant surface area with improved transport. Consequently, utilization of this catalyst support with an ion-conductive interposer and an optimized BPM enabled maintaining CO Faradaic efficiency above 40% at current densities up to 500 mA/cm^2 [70]. Similarly, a recent study optimized the pore alignment and size to enhance *i*-CO_2 activity at the cathode interface and prevent its depletion before adsorption and activation. The optimized nanochannels leveraged non-electrostatic interactions between *i*-CO_2 molecules and the channel walls to effectively trap and retain *i*-CO_2 near the active sites [71]. Three different architectures were analyzed, with the first one relying on 1D transport, the second one consisting of pores between 2–50 nm and 3D transport, and the third geometry that included multi-scale pores with 2–50 nm and <2 nm. The third architecture showed the best performance, enabling a CO Faradaic efficiency of 50% ± 3% at 300 mA/cm^2.

View Article Online
DOI: 10.1039/D6EY00122J

Beyond the limited number of recent RCC studies that have reshaped the magnitude of achieved partial current density through microenvironment control, there are valuable studies in other fields that could be potentially implemented for RCC advancement. We propose that recent findings in CO_2RR [90], the broader area of electrocatalysis [135], and even organic electrochemistry could be beneficial in RCC microenvironment control [29]. For instance, in the design space of redox-active organic compounds, there is promise for compounds that can form CO_2-adducts upon reduction [33,136,137]. Some of these compounds may be integrated with the CO_2RR catalyst in the form of a molecular promoter or be coated at the catalyst surface to bind *i*-CO_2 and prevent the exhaustion effect [138–140]. For instance, it has been demonstrated that indigo-based redox-active molecules attached to Ag nanoparticles provide sites for CO_2 binding that stabilize key intermediates (*COO^- and *COOH), lowering the overpotential for CO production and maintaining CO Faradaic efficiencies above 90% and reaching impressive current densities up to 1,200 mA/cm^2 in a sequential electrolysis configuration [90]. Even though this study utilized CO_2 gas for electrolysis, there could be promising potential if these types of compounds are tested for an RCC configuration.

Despite recent advances, deliberate control of the electrochemical microenvironment in CO_2RR remains underdeveloped, largely due to the time- and resource-intensive nature of such investigations. The microenvironment is inherently multi-scale, with distinct phenomena occurring across adsorption, EDL, diffusion, and bulk regions. RCC performance metrics result from the coupled interplay among transport, solvation, charge distribution, surface adsorption, and reaction pathways spanning these domains [71]. Adjusting a single parameter within one region can induce cascading effects in others because distinct physical and chemical processes govern each scale. Consequently, multi-scale modeling of microenvironment has emerged as a powerful framework to understand the phenomena across interfacial and continuum scales and complement experimental efforts to identify and quantify contributions at each level. Using These multi-scale models could potentially make it possible to construct digital twins, allowing for better understanding and faster optimization of RCC systems.

Figure 7 illustrates different regions in the microenvironment and their characteristic length scales. The proposed strategies to improve RCC metrics can involve one or several regions of microenvironment. Firstly, at the catalyst level, the adsorption region governs metal-induced selectivity and assists with catalyst screening [141]. For instance, the discussed RCC study in Section 4 that developed a CoPc-based catalyst for CO production in an RCC process (Figure S2H), leveraged density functional theory (DFT) to evaluate the electronic structure and electron rich/deficiency of the Co center when different functional groups were present [142]. Using this method, the study narrowed down the functional group selections to carboxylate (COOH), and achieved CO_2RR partial current density of 70 mA/cm^2 at cell voltage of 2.7 V [142].

Secondaly, the strategies to optimize EDL structure and thickness, involve the length scale spanning roughly from several to a few hundred nanometers from the interface (Figure 7). This region is especially important in RCC media due to the complexity of the microenvironment compared to sequential CO_2RR. For instance, amine solutions contain bulky ammonium cations that can increase the thickness of EDL and act as a barrier between *i*-CO_2 and catalyst interface [100,132]. In order to minimize this effect, models in this scale can help to estimate EDL thickness while screening for (i) different types of amines (primary, secondary, tertiary, and stericaly

View Article Online
DOI: 10.1039/D6EY00122J

hindered) [74], and (ii) background electrolyte cations [132], and (iii) surfactants that aim to suppress HER through altering EDL [97].

Thirdly, optimization of substrate through hierarchial porosity and nano-confinement can be facilitated by nano-scale modeling. These strategies are especially proposed to mitigate *i*-CO_2 exhaustion, leading to improvement in partial current density. For example, nanoscale MD has also guided the design of interconnected nano-confining porous catalyst that was used to enhance *i*-CO_2 activity and minimize the *i*-CO_2 exhaustion effect (Figure S3C,E) [71]. Future studies can leverage nanscale MD to assess and screen the different nano- and meso-pore sizes, and find the optimal substrate structure.

Lastly, design of neucleuohilic molecular promoters, which can bind and enrich *i*-CO_2, can also be facilitated by multi-scale modeling through different aspects. The neucleophilicty of the promoter can be finetuned by screening the structure and added functional groups of the promoter. In this process, DFT can help to assess variations of key descriptors (e.g. ΔE_{*CO} and ΔE_{*H}) to optimize activity and selectivity [29,143], and MD can help to analyze the promoter's performance in enriching of *i*-CO_2. This modeling tool was used to evaluate *i*-CO_2 interfacial concentration when PTV scaffold was incorporated to Cu catalyst to trap *i*-CO_2 and avoid its exhaustion (Figure S4C). Future models can use these two tools to optimize neucleophilicty and key descriptors in combination with the large design space of molecular promoters and functional groups constructed from ECC neucleophiles (e.g. quinones, phenazines) and existing CO_2RR promoters [144].

These modeling frameworks can potentially enable constructing RCC digital twins when combined with continuum models. In highly alkaline media, where CO_3^{2-} is the dominant species (e.g. DAC effluent), RCC can become limited by *i*-CO_2 transport in the diffusion layer due to its inherently low concentration. Poisson–Nernst–Planck (PNP) models have been employed to describe transport in this region [145,146]. Relevant parameters include diffusion coefficients (D), concentration gradients (e.g., $C_{i\text{-}CO2}$), pH, and diffusion-layer thickness (δ_{DL}) [146]. Beyond the diffusion layer (at distances greater than ~10^{-5} m from the interface), the bulk layer represents the well-mixed region of the electrolyte where concentration gradients diminish and species distributions approach uniformity. At this scale, macroscopic transport phenomena, such as convection, ionic migration, and ohmic resistance, dominate and collectively influence overall cell performance. Modeling at the diffusion and bulk scales can guide the design of porous catalysts and interposers [70]. Other cell components, such as the membrane and the anode, also benefit from multi-scale modeling [147,148,111]. In particular, analyzing transport in BPMs is crucial for guiding BPM design and fabrication, as BPMs are a major source of voltage loss and thus power consumption in BPM-based RCC systems [111].

View Article Online
DOI: 10.1039/D6EY00122J

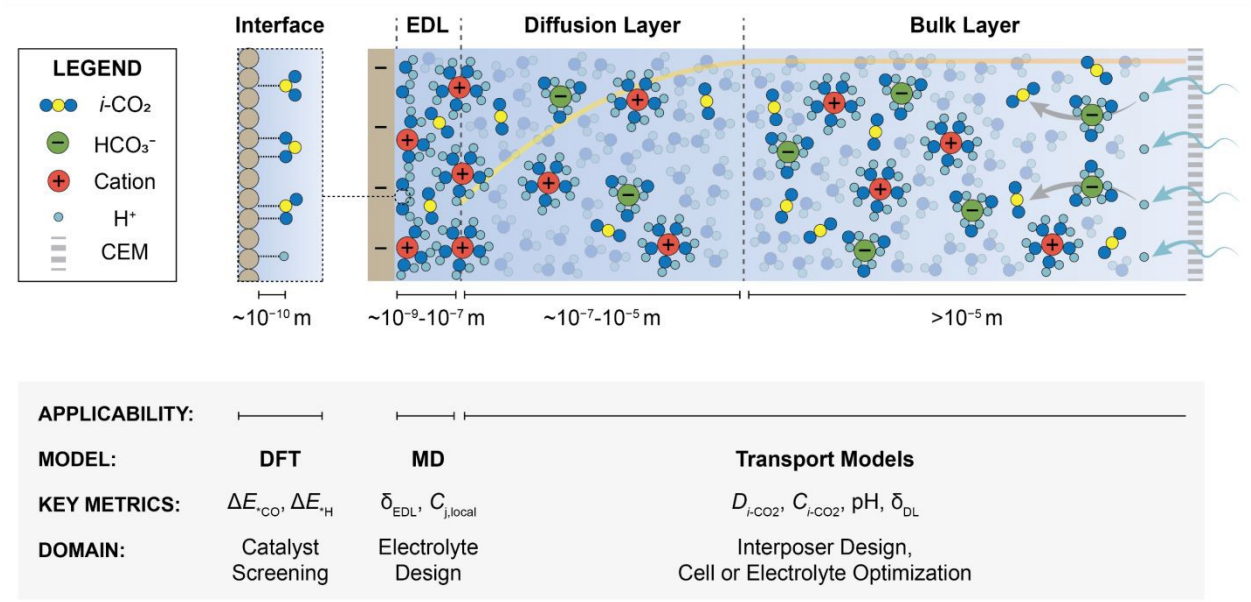

Figure 7. Multi-scale regions and modeling domains in RCC systems. (top) Schematic illustration of the interfacial and transport regions in an RCC catholyte, spanning from the catalyst interface to the bulk electrolyte. The illustration shows HCO_3^- as the CO_2 carrier with a cation exchange membrane (CEM), which facilitates H^+ transfer from the anode to the cathode chamber. The interface (~10^{-10} m) governs adsorption and charge transfer, followed by the electric double layer (EDL, ~10^{-9}–10^{-7} m), where ion accumulation and charge separation occur. Beyond the EDL, the diffusion layer (~10^{-7}–10^{-5} m) exhibits a concentration gradient of reactive species such as *i*-CO_2 (indicated by the yellow profile), which becomes uniform in the bulk region (>10^{-5} m). Together, these regions define the electrochemical microenvironment that controls RCC performance. (bottom) Characteristic modeling approaches and their applicability across scales. Density functional theory (DFT) captures adsorption energetics (ΔE_{*CO}, ΔE_{*H}) relevant to catalyst screening at the interface. Molecular dynamics (MD) simulations describe EDL thickness (δ_{EDL}) and local species concentrations ($C_{j,local}$), informing electrolyte design. Continuum transport models, such as Poisson–Nernst–Planck (PNP) frameworks, resolve macroscopic parameters including diffusion coefficients ($D_{i\text{-}CO2}$), concentration gradients ($C_{i\text{-}CO2}$), pH, and diffusion-layer thickness (δ_{DL}), which guide the design of interposer, cell, and electrolyte optimization.

Overall, the lower CO_2RR partial current densities observed in RCC compared to sequential CO_2RR stem from limitations in *i*-CO_2 generation, transport, and interfacial availability rather than catalyst activity alone. Overcoming these constraints requires a coupled strategy that integrates microenvironment engineering with multi-scale modeling to guide rational design. Microenvironmental tuning, e.g., through electrolyte composition, ionomer architecture, and electrode morphology, can enhance local CO_2 activity and suppress HER. Meanwhile, multi-scale models provide the mechanistic foundation to predict how modifications at the atomic, molecular, and continuum levels impact system-level performance metrics. Advancing RCC toward higher partial current densities will therefore rely on closing this feedback loop between multi-scale modeling and experiment to systematically optimize transport, reaction environments, and cell architectures.

View Article Online
DOI: 10.1039/D6EY00122J

6.3. Stability Challenges in RCC Catalysts and Systems

Despite advancements in reactor design and mechanistic understanding, the stability of RCC systems remains one of the least explored dimensions of this technology. Most published studies report short-term performance metrics such as current density or Faradaic efficiency, but rarely address how these evolve over extended operation. This gap is not surprising, as RCC is still at a relatively low TRL. However, as the field progresses toward scale-up, achieving both catalyst durability and system-level operational stability will be essential for practical implementation.

To date, most stability investigations have focused on amine-based RCC systems, where the complex electrolyte composition can accelerate catalyst degradation [85]. A recent study provided the first mechanistic insight into amine-mediated Cu corrosion, identifying that RCC requires new stability descriptors beyond the ΔE metrics commonly used to explain selectivity in both RCC and sequential CO_2RR [72]. Three interrelated properties of the amine environment were found to govern Cu corrosion: (i) steric effects, where bulky amines hinder electron donation and restrict surface access, slowing corrosion; (ii) Lewis acidity of the conjugate acid (ammonium cations), with amines with lower p*K*a (higher Lewis acidity) intensify corrosion by disrupting protective oxide layers and releasing Cu^{2+} ions; and (iii) nucleophilicity of the nitrogen center, where electron-donating substituents accelerate Cu–amine complexation. These factors introduce a trade-off between catalytic accessibility and corrosion resistance. Amines with high p*K*a inhibit corrosion but impede *i*-CO_2 release, while those with low p*K*a enhance reactivity but destabilize the catalyst. The study proposed the adsorption energy of ammonium cations (ΔE_{NH4+}) as a stability descriptor for Cu-based RCC systems and recommended using amines with high p*K*a and weak ammonium adsorption to minimize corrosion. While this analysis was specific to Cu in amine systems, more recent work on RCC using CoPc-CNT in amino acid medium further showed that in addition to the direct catalyst/amine interactions, long-term stability can be governed by how the capture media regulates local pH and proton flux at the cathode interface [76]. In this study, performance loss was dominated by interfacial degradation processes due to pH-sensitive demetallation [149,150], with EIS data indicating a strong rise in charge transfer resistance and electrolysis analysis revealing dissolved Co, consistent with catalyst decomposition under proton-rich interfacial conditions. Importantly, lowering the glycine concentration shortened lifetime because weaker buffering allowed greater proton flux to the catalyst surface, whereas stronger buffering improved durability but reduced peak CO selectivity by suppressing *i*-CO_2 regeneration and increasing mass-transfer limitations, suggesting a tradeoff between activity and stability [76]. While these analyses were specific to carbamate systems, similar approaches are needed for (bi)carbonate-based RCC, especially for CO formation (as the fovorable product in RCCs), where the chemical environment and degradation pathways could differ substantially. Furthermore, stability studies must extend beyond Cu to other relevant catalysts to assess potential poisoning or degradation by species unique to RCC environments.

Beyond catalyst degradation caused by the capture medium itself, the stability of RCC systems under realistic feed conditions also requires much more attention. In practical operation, impurities such as NOx and SOx can affect RCC already at the capture stage by competing with CO2 for the nucleophilic capture sites in the absorbent. Because these acidic species can consume or deactivate reactive capture sites, they may reduce the effective CO2 absorption capacity and alter

View Article Online
DOI: 10.1039/D6EY00122J

the speciation of the capture liquid delivered to the electrolyzer. In this regard, RCC does not necessarily offer an inherent strategic advantage over sequential systems during the capture step, since both routes may still require impurity pretreatment to preserve sorbent capacity and maintain stable operation.

At the electrochemical conversion stage, the currently available evidence remains limited but suggests that the effect of impurities depends strongly on their chemical form. Initial studies indicate that dissolved SOx-derived species such as SO_3^- and SO_4^- may have negligible impact on Ag-catalyzed CO production, whereas NOx-derived species such as NO_2^- and NO_3^- can lower CO_2RR Faradaic efficiency because they are preferentially reduced. Importantly, the recovery of CO_2RR Faradaic efficiency after switching back to impurity-free electrolyte suggests that, in those cases, the loss in selectivity was not primarily due to irreversible catalyst poisoning. In addition, interfacial engineering strategies such as the use of amphiphilic surfactants have shown promise in maintaining CO_2RR performance in impurity-containing electrolytes. Although these early results are encouraging, they are still insufficient to conclude that RCC generally offers an impurity-tolerant reduction environment. Therefore, future studies must examine how dissolved impurities influence catalyst degradation, sorbent degradation, impurity accumulation, and long-term selectivity under realistic operating conditions.

Beyond catalyst degradation, the long-term operational stability of RCC systems remains largely untested. Repeated cycling between capture and conversion stages can introduce fluctuations in electrolyte composition, pH, and ionic strength, potentially changing CO_2 solubility, *i*-CO_2 transport, and product selectivity over time. Additionally, membrane crossover, electrode flooding, and accumulation of byproducts can progressively degrade cell performance. To enable realistic RCC scale-up from proof-of-concept toward industrially viable carbon capture and conversion systems, future work must include prolonged RCC experiments along with fundamental in-situ characterizations and multi-scale modeling to identify the degradation pathways across electrochemical, chemical, and mechanical domains.

7. CONCLUSIONS

Electrochemical RCC offers a unified route for CO_2 separation and conversion that could simplify carbon management and reduce energy demand relative to conventional sequential routes. Yet, despite its conceptual appeal, RCC remains in an early stage of development, where mechanistic complexity and limited performance metrics constrain its practical advantage. The analyses presented in this Perspective, spanning energetics, electrochemical benchmarking, and techno-economic evaluation, revealed that while RCC can theoretically lower energy consumption by bypassing desorption and compression steps, the realized energy savings remain modest under current conditions due to higher overpotentials and lower partial current densities. Thus, realizing the intrinsic energy benefit of RCC will depend on advancing electrochemical performance through catalyst, membrane, and cell design improvements.

Comparative benchmarking indicated that (bi)carbonate-based RCC systems outperform carbamate-based ones in both activity and product diversity, reflecting the more labile carbon speciation and enhanced availability of *i*-CO_2. However, despite similar operating voltages, RCC

View Article Online
DOI: 10.1039/D6EY00122J

systems still deliver significantly lower partial current densities than sequential CO_2RR, primarily due to *i*-CO_2 transport limits and exhaustion effect near the cathode interface. TEA informed that gaseous products, particularly CO and to some extent C_2H_4, showed near-competitive costs with sequential systems, while liquid products remain unfeasible due to the costly downstream separations. When these economic findings are viewed alongside theoretical EA efficiencies, CO emerges as the most promising near-term product, offering a favorable balance between energy efficiency, system integration, and cost potential. In contrast, products that require larger electron transfers, such as C_{2+}, inherently suffer from low EA efficiency and consequently high capital and operating costs, highlighting the need for targeted rather than generalized RCC development.

Beyond product selection, progress in RCC will require a transition from isolated performance optimization to holistic system integration. Priorities include achieving higher partial current densities through microenvironment engineering and transport control by translating fundamental insights from CO_2RR and electrocatalysis areas into RCC catalyst design, and developing robust, long-term stable materials that can operate in chemically complex capture media. Equally important will be incorporating system-level metrics, such as EA efficiency and integrated TEA frameworks, to ensure that improvements in one subsystem do not compromise overall process viability.

Overall, these findings suggest that RCC is entering a crucial stage of refinement. Its promise has become clear in the proof-of-concept phase so far, but its realization will hinge on coordinated advances that couple molecular-scale understanding with engineering optimization and economic validation. With continued progress in electrochemical performance, system coupling, and materials stability, RCC could evolve from a conceptual innovation into a practical platform for carbon-neutral chemical production and carbon management.

ACKNOWLEDGMENTS

Dr. Rahimi acknowledges the support from the NSF CAREER (Award #: 2338664) and the University of Houston High Priority Area Research Seed Grant (Award #: I0511686).

REFERENCES

1. De Luna P, Hahn C, Higgins D, Jaffer SA, Jaramillo TF, Sargent EH. What would it take for renewably powered electrosynthesis to displace petrochemical processes? Science. 2019;364:eaav3506. doi:10.1126/science.aav3506
2. O'Brien CP, Miao RK, Shayesteh Zeraati A, Lee G, Sargent EH, Sinton D. CO2 Electrolyzers. Chem Rev. 2024;124:3648–93. doi:10.1021/acs.chemrev.3c00206
3. Poust SK. Towards Biochemical Conversion of CO2 to Higher Value Chemicals Using Enzyme Design and Engineered Polyketide Synthases [Internet]. UC Berkeley; 2015 [cited 2025 Jul 29]. Available from: https://escholarship.org/uc/item/8vd4s91k
4. Qiao J, Liu Y, Hong F, Zhang J. A review of catalysts for the electroreduction of carbon dioxide to produce low-carbon fuels. Chem Soc Rev. 2013;43:631–75. doi:10.1039/C3CS60323G
5. Irabien A, Alvarez-Guerra M, Albo J, Dominguez-Ramos A. Electrochemical Conversion of CO2 to Value-Added Products. In: Martínez-Huitle CA, Rodrigo MA, Scialdone O, editors. Electrochemical Water and

View Article Online
DOI: 10.1039/D6EY00122J

Wastewater Treatment [Internet]. Butterworth-Heinemann; 2018 [cited 2025 Jul 29]. p. 29–59. Available from: https://www.sciencedirect.com/science/article/pii/B978012813160200002X doi:10.1016/B978-0-12-813160-2.00002-X

6. Ulmer U, Dingle T, Duchesne PN, Morris RH, Tavasoli A, Wood T, et al. Fundamentals and applications of photocatalytic CO2 methanation. Nat Commun. 2019;10:3169. doi:10.1038/s41467-019-10996-2
7. Kumar B, Llorente M, Froehlich J, Dang T, Sathrum A, Kubiak CP. Photochemical and Photoelectrochemical Reduction of CO2. Annual Review of Physical Chemistry. 2012;63:541–69. doi:10.1146/annurev-physchem-032511-143759
8. Abanades S, Villafan-Vidales HI. CO2 and H2O conversion to solar fuels via two-step solar thermochemical looping using iron oxide redox pair. Chemical Engineering Journal. 2011;175:368–75. doi:10.1016/j.cej.2011.09.124
9. Dardor D, Bhosale R, Gharbia S, AlNouss A, AlMomani F. Solar Thermochemical Conversion of CO2 into C via SnO2/SnO Redox Cycle: A Thermodynamic Study. Vol. 5. 2015;5.
10. Jhong HR "Molly," Ma S, Kenis PJ. Electrochemical conversion of CO2 to useful chemicals: current status, remaining challenges, and future opportunities. Current Opinion in Chemical Engineering. 2013;Nanotechnology / Separation engineering2:191–9. doi:10.1016/j.coche.2013.03.005
11. Jiao L, Yang W, Wan G, Zhang R, Zheng X, Zhou H, et al. Single-Atom Electrocatalysts from Multivariate Metal–Organic Frameworks for Highly Selective Reduction of CO2 at Low Pressures. Angewandte Chemie International Edition. 2020;59:20589–95. doi:10.1002/anie.202008787
12. Wen X, Gao D, Wang G. Direct Electrochemical Conversion of CO2 from Industrial Flue Gases. ChemSusChem. 2025;18:e202402438. doi:10.1002/cssc.202402438
13. Cobb SJ, Dharani AM, Oliveira AR, Pereira IAC, Reisner E. Carboxysome-Inspired Electrocatalysis using Enzymes for the Reduction of CO2 at Low Concentrations. Angewandte Chemie International Edition. 2023;62:e202218782. doi:10.1002/anie.202218782
14. Van Daele S, Hintjens L, Hoekx S, Bohlen B, Neukermans S, Daems N, et al. How flue gas impurities affect the electrochemical reduction of CO2 to CO and formate. Applied Catalysis B: Environmental. 2024;341:123345. doi:10.1016/j.apcatb.2023.123345
15. Hao S, Elgazzar A, Zhang SK, Wi TU, Chen FY, Feng Y, et al. Acid-humidified CO2 gas input for stable electrochemical CO2 reduction reaction. Science. 2025;388:eadr3834. doi:10.1126/science.adr3834
16. Ko BH, Hasa B, Shin H, Jeng E, Overa S, Chen W, et al. The impact of nitrogen oxides on electrochemical carbon dioxide reduction. Nat Commun. 2020;11:5856. doi:10.1038/s41467-020-19731-8
17. Luc W, Ko BH, Kattel S, Li S, Su D, Chen JG, et al. SO2-Induced Selectivity Change in CO2 Electroreduction. Journal of the American Chemical Society. 2019. Located at: world. doi:10.1021/jacs.9b03215
18. Renfrew SE, Starr DE, Strasser P. Electrochemical Approaches toward CO2 Capture and Concentration. ACS Catal. 2020;10:13058–74. doi:10.1021/acscatal.0c03639
19. Bui M, Adjiman CS, Bardow A, Anthony EJ, Boston A, Brown S, et al. Carbon capture and storage (CCS): the way forward. Energy Environ Sci. 2018;11:1062–176. doi:10.1039/C7EE02342A
20. Refaie A, Afshari M, Tapia V, La Plante E, Jassby D, Sant G, et al. Comparative assessment of United States coastal hubs for large scale electrochemical marine carbon dioxide removal. Commun Sustain. 2026;1:33. doi:10.1038/s44458-026-00035-9
21. Hassan A, Refaie A, Aleta P, Afshari M, Kalantari E, Fang Y, et al. Reviving the absorbent chemistry of electrochemically mediated amine regeneration for improved point source carbon capture. Chemical Engineering Journal. 2024;484:149566. doi:10.1016/j.cej.2024.149566
22. Hassan A, Afshari M, Rahimi M. A Membraneless Electrochemically Mediated Amine Regeneration for Carbon Capture. Nat Commun. 2025;16:6333. doi:10.1038/s41467-025-61525-3

View Article Online
DOI: 10.1039/D6EY00122J

23. Rahimi M, Khurram A, Hatton TA, Gallant B. Electrochemical carbon capture processes for mitigation of CO2 emissions. Chem Soc Rev. 2022;51:8676–95. doi:10.1039/D2CS00443G

24. Sharifian R, Wagterveld RM, Digdaya IA, Xiang C, Vermaas DA. Electrochemical carbon dioxide capture to close the carbon cycle. Energy Environ Sci. 2021;14:781–814. doi:10.1039/D0EE03382K

25. Zito AM, Clarke LE, Barlow JM, Bím D, Zhang Z, Ripley KM, et al. Electrochemical Carbon Dioxide Capture and Concentration. Chem Rev. 2023;123:8069–98. doi:10.1021/acs.chemrev.2c00681

26. Liu Y, Ye HZ, Diederichsen KM, Van Voorhis T, Hatton TA. Electrochemically mediated carbon dioxide separation with quinone chemistry in salt-concentrated aqueous media. Nat Commun. 2020;11:2278. doi:10.1038/s41467-020-16150-7

27. Barlow JM, Clarke LE, Zhang Z, Bím D, Ripley KM, Zito A, et al. Molecular design of redox carriers for electrochemical CO2 capture and concentration. Chem Soc Rev. 2022;51:8415–33. doi:10.1039/D2CS00367H

28. Barlow JM, Yang JY. Oxygen-Stable Electrochemical CO2 Capture and Concentration with Quinones Using Alcohol Additives. J Am Chem Soc. 2022;144:14161–9. doi:10.1021/jacs.2c04044

29. Li X, Zhao X, Liu Y, Hatton TA, Liu Y. Redox-tunable Lewis bases for electrochemical carbon dioxide capture. Nat Energy. 2022;7:1065–75. doi:10.1038/s41560-022-01137-z

30. Eisaman MD, Alvarado L, Larner D, Wang P, Garg B, Littau KA. CO2 separation using bipolar membrane electrodialysis. Energy Environ Sci. 2011;4:1319–28. doi:10.1039/C0EE00303D

31. Jin S, Wu M, Gordon RG, Aziz MJ, Kwabi DG. pH swing cycle for CO2 capture electrochemically driven through proton-coupled electron transfer. Energy Environ Sci. 2020;13:3706–22. doi:10.1039/D0EE01834A

32. Seo H, Rahimi M, Hatton TA. Electrochemical Carbon Dioxide Capture and Release with a Redox-Active Amine. J Am Chem Soc. 2022;144:2164–70. doi:10.1021/jacs.1c10656

33. Pang S, Jin S, Yang F, Alberts M, Li L, Xi D, et al. A phenazine-based high-capacity and high-stability electrochemical CO2 capture cell with coupled electricity storage. Nat Energy. 2023;8:1126–36. doi:10.1038/s41560-023-01347-z

34. Afshari M, Refaie A, Aleta P, Hassan A, Rahimi M. A Vanadium Redox Flow Process for Carbon Capture and Energy Storage. ACS EST Eng. 2025;5:1099–110. doi:10.1021/acsestengg.4c00631

35. Refaie A, Hassan A, Afshari M, Fang Y, Rahimi M. Electrochemical Carbon Capture via Engineered Polarized Liquid–Liquid Interfaces. ACS Electrochem. 2026. doi:10.1021/acselectrochem.6c00096

36. Rahimi M, Catalini G, Hariharan S, Wang M, Puccini M, Hatton TA. Carbon Dioxide Capture Using an Electrochemically Driven Proton Concentration Process. Cell Reports Physical Science. 2020;1:100033. doi:10.1016/j.xcrp.2020.100033

37. Afshari M, Hashemi SM, Powell JB, Hatton TA, Rahimi M. Economics of Scaling Up Electrochemical Carbon Capture Processes. ChemRxiv. 2026. doi:10.26434/chemrxiv.10002103/v1

38. Wang M, Rahimi M, Kumar A, Hariharan S, Choi W, Hatton TA. Flue gas CO2 capture via electrochemically mediated amine regeneration: System design and performance. Applied energy. 2019;255:113879.

39. Rahimi M, Diederichsen KM, Ozbek N, Wang M, Choi W, Hatton TA. An Electrochemically Mediated Amine Regeneration Process with a Mixed Absorbent for Postcombustion CO2 Capture. Environ Sci Technol. 2020;54:8999–9007. doi:10.1021/acs.est.0c02595

40. C. Stern M, Simeon F, Herzog H, Alan Hatton T. Post- combustion carbon dioxide capture using electrochemically mediated amine regeneration. Energy & Environmental Science. 2013;6:2505–17. doi:10.1039/C3EE41165F

41. Rahimi M, Zucchelli F, Puccini M, Alan Hatton T. Improved CO2 Capture Performance of Electrochemically Mediated Amine Regeneration Processes with Ionic Surfactant Additives. ACS Appl Energy Mater. 2020;3:10823–30. doi:10.1021/acsaem.0c01859

42. Aleta P, Refaie A, Afshari M, Hassan A, Rahimi M. Direct ocean capture: the emergence of electrochemical processes for oceanic carbon removal. Energy Environ Sci. 2023;16:4944–67. doi:10.1039/D3EE01471A

View Article Online
DOI: 10.1039/D6EY00122J

43. Rahimi M, Catalini G, Puccini M, Alan Hatton T. Bench-scale demonstration of CO 2 capture with an electrochemically driven proton concentration process. RSC Advances. 2020;10:16832–43. doi:10.1039/D0RA02450C

44. Li M, Irtem E, Iglesias van Montfort HP, Abdinejad M, Burdyny T. Energy comparison of sequential and integrated CO2 capture and electrochemical conversion. Nat Commun. 2022;13:5398. doi:10.1038/s41467-022-33145-8

45. Lee H, Kwon S, Park N, Cha SG, Lee E, Kong TH, et al. Scalable Low-Temperature CO2 Electrolysis: Current Status and Outlook. JACS Au. 2024;4:3383–99. doi:10.1021/jacsau.4c00583

46. Zhao Y, Hao L, Ozden A, Liu S, Miao RK, Ou P, et al. Conversion of CO2 to multicarbon products in strong acid by controlling the catalyst microenvironment. Nat Synth. 2023;2:403–12. doi:10.1038/s44160-022-00234-x

47. García de Arquer FP, Dinh CT, Ozden A, Wicks J, McCallum C, Kirmani AR, et al. CO2 electrolysis to multicarbon products at activities greater than 1 A cm−2. Science. 2020;367:661–6. doi:10.1126/science.aay4217

48. Wakerley D, Lamaison S, Wicks J, Clemens A, Feaster J, Corral D, et al. Gas diffusion electrodes, reactor designs and key metrics of low-temperature CO2 electrolysers. Nat Energy. 2022;7:130–43. doi:10.1038/s41560-021-00973-9

49. Zhong M, Tran K, Min Y, Wang C, Wang Z, Dinh CT, et al. Accelerated discovery of CO2 electrocatalysts using active machine learning. Nature. 2020;581:178–83. doi:10.1038/s41586-020-2242-8

50. Li Z, Xu Y, Li X, Foley GDY, Lin DZ, Zhang L, et al. Multifunctional Binding Interface Drives Near-Unity CO Selectivity in Acidic CO2 Electrolysis. Angewandte Chemie International Edition. n/a:e202514111. doi:10.1002/anie.202514111

51. Pimlott DJD, Kim Y, Berlinguette CP. Reactive Carbon Capture Enables CO2 Electrolysis with Liquid Feedstocks. Acc Chem Res. 2024;57:1007–18. doi:10.1021/acs.accounts.3c00571

52. Garcia JA, Villen-Guzman M, Rodriguez-Maroto JM, Paz-Garcia JM. Technical analysis of CO2 capture pathways and technologies. Journal of Environmental Chemical Engineering. 2022;10:108470. doi:10.1016/j.jece.2022.108470

53. Borhani TN, Abbasi MR, Hosseinpour M, Salimi M, Afkhamipour M, Oko E, et al. CO2 absorption-desorption cycles: Progress, gaps, and future. Carbon Capture Science & Technology. 2024;13:100325. doi:10.1016/j.ccst.2024.100325

54. Orella MJ, Brown SM, Leonard ME, Román-Leshkov Y, Brushett FR. A General Technoeconomic Model for Evaluating Emerging Electrolytic Processes. Energy Technology. 2020;8:1900994. doi:10.1002/ente.201900994

55. Venkataraman A, Song H, Brandão VD, Ma C, Casajus MS, Fernandez Otero CA, et al. Process and techno-economic analyses of ethylene production by electrochemical reduction of aqueous alkaline carbonates. Nat Chem Eng. 2024;1:710–23. doi:10.1038/s44286-024-00137-y

56. Shen K, Cheng D, Reyes-Lopez E, Jang J, Sautet P, Morales-Guio CG. On the origin of carbon sources in the electrochemical upgrade of CO2 from carbon capture solutions. Joule. 2023;7:1260–76. doi:10.1016/j.joule.2023.05.010

57. Xiao YC, Sun SS, Zhao Y, Miao RK, Fan M, Lee G, et al. Reactive capture of CO2 via amino acid. Nat Commun. 2024;15:7849. doi:10.1038/s41467-024-51908-3

58. Jerng SE, Gallant BM. Electrochemical reduction of CO2 in the captured state using aqueous or nonaqueous amines. iScience. 2022;25. doi:10.1016/j.isci.2022.104558 PubMed PMID: 35747389.

59. Khurram A, Yan L, Yin Y, Zhao L, Gallant BM. Promoting Amine-Activated Electrochemical CO2 Conversion with Alkali Salts. J Phys Chem C. 2019;123:18222–31. doi:10.1021/acs.jpcc.9b04258

60. Lee G, Li YC, Kim JY, Peng T, Nam DH, Sedighian Rasouli A, et al. Electrochemical upgrade of CO2 from amine capture solution. Nat Energy. 2021;6:46–53. doi:10.1038/s41560-020-00735-z

View Article Online
DOI: 10.1039/D6EY00122J

61. Bruggeman DF, Rothenberg G, Garcia AC. Investigating proton shuttling and electrochemical mechanisms of amines in integrated CO2 capture and utilization. Nat Commun. 2024;15:9207. doi:10.1038/s41467-024-53543-4

62. Kim Y, Lees EW, Donde C, Jewlal AML, Waizenegger CEB, Hepcée BMW de, et al. Integrated CO2 capture and conversion to form syngas. Joule. 2024;8:3106–25. doi:10.1016/j.joule.2024.10.010

63. Leverick G, Bernhardt EM, Ismail AI, Law JH, Arifutzzaman A, Aroua MK, et al. Uncovering the Active Species in Amine-Mediated CO2 Reduction to CO on Ag. ACS Catal. 2023;13:12322–37. doi:10.1021/acscatal.3c02500

64. Kowalski RM, Banerjee A, Yue C, Gracia SG, Cheng D, Morales-Guio CG, et al. Electroreduction of Captured CO2 on Silver Catalysts: Influence of the Capture Agent and Proton Source. J Am Chem Soc. 2024;146:20728–41. doi:10.1021/jacs.4c03915

65. Sullivan I, Goryachev A, Digdaya IA, Li X, Atwater HA, Vermaas DA, et al. Coupling electrochemical CO2 conversion with CO2 capture. Nat Catal. 2021;4:952–8. doi:10.1038/s41929-021-00699-7

66. Li M, Yang K, Abdinejad M, Zhao C, Burdyny T. Advancing integrated CO2 electrochemical conversion with amine-based CO2 capture: a review. Nanoscale. 2022;14:11892–908. doi:10.1039/D2NR03310K

67. Xia Q, Zhang K, Zheng T, An L, Xia C, Zhang X. Integration of CO2 Capture and Electrochemical Conversion. ACS Energy Lett. 2023;8:2840–57. doi:10.1021/acsenergylett.3c00738

68. Namdari M, Kim Y, Pimlott DJD, Jewlal AML, Berlinguette CP. Reactive carbon capture using electrochemical reactors. Chem Soc Rev. 2025;54:590–600. doi:10.1039/D4CS00834K

69. Banerjee A, Morales-Guio CG. Integrated CO2 capture and electrochemical conversion: coupled effects of transport, kinetics and thermodynamics in the direct reduction of captured-CO2 adducts. EES Catal. 2025;3:205–34. doi:10.1039/D4EY00285G

70. Liu H, Shin H, Li XY, Su G, Ou P, Wang Y, et al. Hierarchically porous carbon supports enable efficient syngas production in electrified reactive capture. Energy Environ Sci. 2025;18:6628–40. doi:10.1039/D5EE00094G

71. Liu H, An L, Wang P, Yu C, Zhang J, Shin H, et al. Interconnected nanoconfining pore networks enhance catalyst CO2 interaction in electrified reactive capture. Nat Commun. 2025;16:6185. doi:10.1038/s41467-025-61407-8

72. Choi J, Banerjee A, Ross RD, Zhang Z, Chiu S, Sacci RL, et al. Amine Structure Governs Corrosion Rates of Copper Catalysts in Electrochemical Reactive Capture of CO2. J Phys Chem C. 2025;129:16009–19. doi:10.1021/acs.jpcc.5c03178

73. Lorenzutti F, Seemakurthi RR, Johnson EF, Morandi S, Nikačević P, López N, et al. Microenvironment effects in electrochemical CO2 reduction from first-principles multiscale modelling. Nat Catal. 2025;8:905–18. doi:10.1038/s41929-025-01399-2

74. Li P, Mao Y, Shin H, Yang Q, Cheng X, Li Y, et al. Tandem amine scrubbing and CO2 electrolysis via direct piperazine carbamate reduction. Nat Energy. 2025;1–12. doi:10.1038/s41560-025-01869-8

75. Xu T, Yin G, Wang F, Yang F, Xu J, Ye J, et al. Creating a Microenvironment in an Amine Solution for Integrated CO2 Capture and Electroreduction. ACS Catal. 2025;17133–43. doi:10.1021/acscatal.5c05334

76. Xiao YC, Guo Z, Wang R, Li F, Sun SS, Liu M, et al. Solvent tuning regulates proton flux to extend stability in reactive CO2 capture and electrolysis. Chem Catalysis. 2026;0. doi:10.1016/j.checat.2026.101694

77. Malik K, Singh S, Basu S, Verma A. Electrochemical reduction of CO2 for synthesis of green fuel. WIREs Energy and Environment. 2017;6:e244. doi:10.1002/wene.244

78. Voiry D, Shin HS, Loh KP, Chhowalla M. Low-dimensional catalysts for hydrogen evolution and CO2 reduction. Nat Rev Chem. 2018;2:0105. doi:10.1038/s41570-017-0105

79. Lees EW, Mowbray BAW, Parlane FGL, Berlinguette CP. Gas diffusion electrodes and membranes for CO2 reduction electrolysers. Nat Rev Mater. 2022;7:55–64. doi:10.1038/s41578-021-00356-2

80. Costentin C, Robert M, Savéant JM. Catalysis of the electrochemical reduction of carbon dioxide. Chem Soc Rev. 2013;42:2423–36. doi:10.1039/C2CS35360A

View Article Online
DOI: 10.1039/D6EY00122J

81. Sheng W, Kattel S, Yao S, Yan B, Liang Z, Hawxhurst CJ, et al. Electrochemical reduction of CO2 to synthesis gas with controlled CO/H2 ratios. Energy Environ Sci. 2017;10:1180–5. doi:10.1039/C7EE00071E

82. Bagger A, Ju W, Varela AS, Strasser P, Rossmeisl J. Electrochemical CO2 Reduction: A Classification Problem. ChemPhysChem. 2017;18:3266–73. doi:10.1002/cphc.201700736

83. Bard AJ. Standard Potentials in Aqueous Solution. New York: Routledge; 2017. 848 p. doi:10.1201/9780203738764

84. Bagger A, Ju W, Varela AS, Strasser P, Rossmeisl J. Electrochemical CO2 Reduction: Classifying Cu Facets. ACS Catal. 2019;9:7894–9. doi:10.1021/acscatal.9b01899

85. Choi J, Chiu S, Banerjee A, Sacci RL, Veith GM, Stieber C, et al. Corrosion and Enhanced Hydrogen Evolution in Electrochemical Reduction of Ammonium Carbamate on Transition Metal Surfaces. J Phys Chem Lett. 2024;15:8007–17. doi:10.1021/acs.jpclett.4c01638

86. Nitopi S, Bertheussen E, Scott SB, Liu X, Engstfeld AK, Horch S, et al. Progress and Perspectives of Electrochemical CO2 Reduction on Copper in Aqueous Electrolyte. Chem Rev. 2019;119:7610–72. doi:10.1021/acs.chemrev.8b00705

87. Zhang H, Gao J, Raciti D, Hall AS. Promoting Cu-catalysed CO2 electroreduction to multicarbon products by tuning the activity of H2O. Nat Catal. 2023;6:807–17. doi:10.1038/s41929-023-01010-6

88. Tajalli P, Omidiyan M, Rahimi MM, Lee TR. Exploring the potential of transition-metal-based hollow micro- and nanoparticles in supercapacitor electrodes. Materials Today Sustainability. 2024;26:100733. doi:10.1016/j.mtsust.2024.100733

89. Agarwal VG, Haussener S. Quantifying mass transport limitations in a microfluidic CO2 electrolyzer with a gas diffusion cathode. Commun Chem. 2024;7:47. doi:10.1038/s42004-024-01122-5

90. Li Z, Li X, Wang R, Campos Mata A, Gerke CS, Xiang S, et al. Electro-activated indigos intensify ampere-level CO2 reduction to CO on silver catalysts. Nat Commun. 2025;16:3206. doi:10.1038/s41467-025-58593-w

91. Li X, Kang W, Fan X, Tan X, Masa J, Robertson AW, et al. Electrochemical CO2 reduction to liquid fuels: Mechanistic pathways and surface/interface engineering of catalysts and electrolytes. Innovation. 2025;6. doi:10.1016/j.xinn.2025.100807

92. Detz RJ, Ferchaud CJ, Kalkman AJ, Kemper J, Sánchez-Martínez C, Saric M, et al. Electrochemical CO2 conversion technologies: state-of-the-art and future perspectives. Sustainable Energy Fuels. 2023;7:5445–72. doi:10.1039/D3SE00775H

93. CO 2 for a clean performance: Rheticus research project enters phase 2 [Internet]. [cited 2025 Aug 19]. Available from: https://www.siemens-energy.com/us/en/home/press-releases/research-project-rheticus.html

94. Jenkins S. OCO Chem commissions first pilot plant for CO2 electrolysis. Chemical Engineering [Internet]. 2025 [cited 2025 Aug 19]. Available from: https://www.chemengonline.com/oco-chem-commissions-first-pilot-plant-for-co2-electrolysis/

95. Amatore C, Saveant JM. Mechanism and kinetic characteristics of the electrochemical reduction of carbon dioxide in media of low proton availability. J Am Chem Soc. 1981;103:5021–3. doi:10.1021/ja00407a008

96. Jiang TW, Jiang K, Cai WB. Electrochemical CO2 reduction on Pd-based electrodes: from mechanism understanding to rational catalyst design. J Mater Chem A. 2024;12:21515–30. doi:10.1039/D4TA02379J

97. Chen L, Li F, Zhang Y, Bentley CL, Horne M, Bond AM, et al. Electrochemical Reduction of Carbon Dioxide in a Monoethanolamine Capture Medium. ChemSusChem. 2017;10:4109–18. doi:10.1002/cssc.201701075

98. Bohlen B, Daems N, Su Z, Chen A, Lipkowski J, Breugelmans T. In Situ Spectroelectrochemical Study of Acetate Formation by CO2 Reduction Using Bi Catalyst in Amine-Based Capture Solution. ChemSusChem. 2024;17:e202400437. doi:10.1002/cssc.202400437

99. Neves-Garcia T, Hasan M, Zhu Q, Li J, Jiang Z, Liang Y, et al. Integrated Carbon Dioxide Capture by Amines and Conversion to Methane on Single-Atom Nickel Catalysts. J Am Chem Soc. 2024;146:31633–46. doi:10.1021/jacs.4c09744

View Article Online
DOI: 10.1039/D6EY00122J

100. Kim JH, Jang H, Bak G, Choi W, Yun H, Lee E, et al. The insensitive cation effect on a single atom Ni catalyst allows selective electrochemical conversion of captured CO2 in universal media. Energy Environ Sci. 2022;15:4301–12. doi:10.1039/D2EE01825J

101. Bhattacharya M, Sebghati S, Vercella YM, Saouma CT. Electrochemical Reduction of Carbamates and Carbamic Acids: Implications for Combined Carbon Capture and Electrochemical CO2 Recycling. J Electrochem Soc. 2020;167:086507. doi:10.1149/1945-7111/ab8ed0

102. Khakpour R, Laasonen K, Busch M. Selectivity of CO2, carbonic acid and bicarbonate electroreduction over Iron-porphyrin catalyst: A DFT study. Electrochimica Acta. 2023;442:141784. doi:10.1016/j.electacta.2022.141784

103. Khakpour R, Lindberg D, Laasonen K, Busch M. CO2 or Carbonates – What is the Active Species in Electrochemical CO2 Reduction over Fe-Porphyrin? ChemCatChem. 2023;15:e202201671. doi:10.1002/cctc.202201671

104. Obasanjo CA, Gao G, Crane J, Golovanova V, García de Arquer FP, Dinh CT. High-rate and selective conversion of CO2 from aqueous solutions to hydrocarbons. Nat Commun. 2023;14:3176. doi:10.1038/s41467-023-38963-y

105. Lee G, Rasouli AS, Lee BH, Zhang J, Won DH, Xiao YC, et al. CO2 electroreduction to multicarbon products from carbonate capture liquid. Joule. 2023;7:1277–88. doi:10.1016/j.joule.2023.05.003

106. Pérez-Gallent E, Vankani C, Sánchez-Martínez C, Anastasopol A, Goetheer E. Integrating CO2 Capture with Electrochemical Conversion Using Amine-Based Capture Solvents as Electrolytes. Ind Eng Chem Res. 2021;60:4269–78. doi:10.1021/acs.iecr.0c05848

107. Almajed HM, Kas R, Brimley P, Crow AM, Somoza-Tornos A, Hodge BM, et al. Closing the Loop: Unexamined Performance Trade-Offs of Integrating Direct Air Capture with (Bi)carbonate Electrolysis. ACS Energy Lett. 2024;9:2472–83. doi:10.1021/acsenergylett.4c00807

108. Xiao YC, Gabardo CM, Liu S, Lee G, Zhao Y, O'Brien CP, et al. Direct carbonate electrolysis into pure syngas. EES Catal. 2023;1:54–61. doi:10.1039/D2EY00046F

109. Zhang Z, Lees EW, Habibzadeh F, Salvatore DA, Ren S, Simpson GL, et al. Porous metal electrodes enable efficient electrolysis of carbon capture solutions. Energy Environ Sci. 2022;15:705–13. doi:10.1039/D1EE02608A

110. Zhang Z, Lees EW, Ren S, Mowbray BAW, Huang A, Berlinguette CP. Conversion of Reactive Carbon Solutions into CO at Low Voltage and High Carbon Efficiency. ACS Cent Sci. 2022;8:749–55. doi:10.1021/acscentsci.2c00329

111. Bui JC, Lees EW, Marin DH, Stovall TN, Chen L, Kusoglu A, et al. Multi-scale physics of bipolar membranes in electrochemical processes. Nat Chem Eng. 2024;1:45–60. doi:10.1038/s44286-023-00009-x

112. Zhang Z, Kummeth AL, Yang JY, Alexandrova AN. Inverse molecular design of alkoxides and phenoxides for aqueous direct air capture of CO2. Proceedings of the National Academy of Sciences. 2022;119:e2123496119. doi:10.1073/pnas.2123496119

113. Jouny M, Luc W, Jiao F. General Techno-Economic Analysis of CO2 Electrolysis Systems. Ind Eng Chem Res. 2018;57:2165–77. doi:10.1021/acs.iecr.7b03514

114. Spurgeon JM, Kumar B. A comparative technoeconomic analysis of pathways for commercial electrochemical CO2 reduction to liquid products. Energy Environ Sci. 2018;11:1536–51. doi:10.1039/C8EE00097B

115. Kim Y, Namdari M, Jewlal AML, Chen Y, Pimlott DJD, Stolar M, et al. Economic Viability of Integrated CO2 Capture and Conversion. ACS Energy Lett. 2025;10:403–9. doi:10.1021/acsenergylett.4c02852

116. Badreldin A, Li Y. A critical appraisal of advances in integrated CO 2 capture and electrochemical conversion. Chemical Science. 2025;16:2483–513. doi:10.1039/D4SC06642A

117. Srimuk P, Su X, Yoon J, Aurbach D, Presser V. Charge-transfer materials for electrochemical water desalination, ion separation and the recovery of elements. Nat Rev Mater. 2020;5:517–38. doi:10.1038/s41578-020-0193-1

View Article Online
DOI: 10.1039/D6EY00122J

118. Mutch GA. Electrochemical separation processes for future societal challenges. CR-PHYS-SC. 2022;3. doi:10.1016/j.xcrp.2022.100844

119. Cath TY, Childress AE, Elimelech M. Forward osmosis: Principles, applications, and recent developments. Journal of Membrane Science. 2006;281:70–87. doi:10.1016/j.memsci.2006.05.048

120. Park HB, Kamcev J, Robeson LM, Elimelech M, Freeman BD. Maximizing the right stuff: The trade-off between membrane permeability and selectivity. Science. 2017;356:eaab0530. doi:10.1126/science.aab0530

121. Kibria MG, Edwards JP, Gabardo CM, Dinh CT, Seifitokaldani A, Sinton D, et al. Electrochemical CO2 Reduction into Chemical Feedstocks: From Mechanistic Electrocatalysis Models to System Design. Advanced Materials. 2019;31:1807166. doi:10.1002/adma.201807166

122. Bushuyev OS, Luna PD, Dinh CT, Tao L, Saur G, Lagemaat J van de, et al. What Should We Make with CO2 and How Can We Make It? Joule. 2018;2:825–32. doi:10.1016/j.joule.2017.09.003

123. Spurgeon JM, Theaker N, Phipps CA, Uttarwar SS, Grapperhaus CA. Comparative Technoeconomic Analysis of Pathways for Electrochemical Reduction of CO2 with Methanol to Produce Methyl Formate. ACS Sustainable Chem Eng. 2022;10:12882–94. doi:10.1021/acssuschemeng.2c04362

124. Herron JA, Maravelias CT. Assessment of Solar-to-Fuels Strategies: Photocatalysis and Electrocatalytic Reduction. Energy Technology. 2016;4:1369–91. doi:10.1002/ente.201600163

125. Ramdin M, Morrison ART, de Groen M, van Haperen R, de Kler R, Irtem E, et al. High-Pressure Electrochemical Reduction of CO2 to Formic Acid/Formate: Effect of pH on the Downstream Separation Process and Economics. Ind Eng Chem Res. 2019;58:22718–40. doi:10.1021/acs.iecr.9b03970

126. Rumayor M, Dominguez-Ramos A, Perez P, Irabien A. A techno-economic evaluation approach to the electrochemical reduction of CO2 for formic acid manufacture. Journal of CO2 Utilization. 2019;34:490–9. doi:10.1016/j.jcou.2019.07.024

127. Jewlal AML, Kim Y, Crescenzo GV, Berlinguette CP. Go with CO: A Case for Targeting Carbon Monoxide As a Reactive Carbon Capture Product. ACS Energy Lett. 2025;10:2498–502. doi:10.1021/acsenergylett.4c03584

128. Shaw RA, Hatton TA. Electrochemical CO2 capture thermodynamics. International Journal of Greenhouse Gas Control. 2020;95:102878. doi:10.1016/j.ijggc.2019.102878

129. Jing Y, Amini K, Xi D, Jin S, Alfaraidi AM, Kerr EF, et al. Electrochemically Induced CO2 Capture Enabled by Aqueous Quinone Flow Chemistry. ACS Energy Lett. 2024;9:3526–35. doi:10.1021/acsenergylett.4c01235

130. Liu A, Musgrave CB, Li X, Goddard WA, Liu Y. Non-aqueous alkoxide-mediated electrochemical carbon capture. Nat Energy. 2024;9:1415–26. doi:10.1038/s41560-024-01614-7

131. Zhang J, Cao Y, Ou P, Lee G, Zhao Y, Liu S, et al. A redox-active polymeric network facilitates electrified reactive-capture electrosynthesis to multi-carbon products from dilute CO2-containing streams. Nat Commun. 2025;16:3553. doi:10.1038/s41467-025-58756-9

132. Lee G, Li YC, Kim JY, Peng T, Nam DH, Sedighian Rasouli A, et al. Electrochemical upgrade of CO2 from amine capture solution. Nat Energy. 2020;6:46–53. doi:10.1038/s41560-020-00735-z

133. Xu T, Yin G, Wang F, Yang F, Xu J, Ye J, et al. Creating a Microenvironment in an Amine Solution for Integrated CO2 Capture and Electroreduction. ACS Catal. 2025;17133–43. doi:10.1021/acscatal.5c05334

134. Chen L, Li F, Zhang Y, Bentley CL, Horne M, Bond AM, et al. Electrochemical Reduction of Carbon Dioxide in a Monoethanolamine Capture Medium. ChemSusChem. 2017;10:4109–18. doi:10.1002/cssc.201701075

135. Lu P, Singh S, Gonzalez A, Gadikota G. Tunable Electrochemical Reactive Carbon Dioxide Capture and Conversion to Produce Syngas Using Highly Dispersed Nickel Catalyst. ACS Sustainable Chem Eng. 2025;13:5963–73. doi:10.1021/acssuschemeng.5c00653

136. Le PH, Liu A, Zasada LB, Geary J, Kamin AA, Rollins DS, et al. Nitrogen-Rich Conjugated Macrocycles: Synthesis, Conductivity, and Application in Electrochemical CO2 Capture. Angewandte Chemie International Edition. n/a:e202421822. doi:10.1002/anie.202421822

View Article Online
DOI: 10.1039/D6EY00122J

137. Li X, Mathur A, Liu A, Liu Y. Electrifying Carbon Capture by Developing Nanomaterials at the Interface of Molecular and Process Engineering. Acc Chem Res. 2023;56:2763–75. doi:10.1021/acs.accounts.3c00321

138. Sanz-Pérez ES, Murdock CR, Didas SA, Jones CW. Direct Capture of CO2 from Ambient Air. Chem Rev. 2016;116:11840–76. doi:10.1021/acs.chemrev.6b00173

139. Sun JW, Yu T, Wu H, Zhu M, Chen A, Lian C, et al. Direct oxygen-containing simulated flue gas electrolysis over amine-confined Ag catalyst in a flow cell. Chem Catalysis. 2024;4. doi:10.1016/j.checat.2024.100923

140. Li Z, Xu Y, Li X, Foley GDY, Lin DZ, Zhang L, et al. Multifunctional Binding Interface Drives Near-Unity CO Selectivity in Acidic CO2 Electrolysis. Angewandte Chemie International Edition. n/a:e202514111. doi:10.1002/anie.202514111

141. Rafie SF, Tamtaji M, Rahimi M, Nunna PRT, Abu-Zahra N. Steered rare event and classical MD combined with quantum DFT for multiscale mechanistic modeling of CO2 capture by amine-based solvents. Journal of Environmental Chemical Engineering. 2025;13:119470. doi:10.1016/j.jece.2025.119470

142. Zhou B, Liu H, Su G, Shin H, Li XY, Ze H, et al. Electrosynthesis of CO from an electrically pH-shifted DAC post-capture liquid using a catalyst:support amide linkage. Joule. 2025;9:101883. doi:10.1016/j.joule.2025.101883

143. Li Z, Li X, Wang R, Campos Mata A, Gerke CS, Xiang S, et al. Electro-activated indigos intensify ampere-level CO2 reduction to CO on silver catalysts. Nat Commun. 2025;16:3206. doi:10.1038/s41467-025-58593-w

144. Schreier M, Kenis P, Che F, Hall AS. Trends in Electrocatalysis: The Microenvironment Moves to Center Stage. ACS Energy Lett. 2023;8:3935–40. doi:10.1021/acsenergylett.3c01623

145. Zhu X, Huang J, Eikerling M. Electrochemical CO2 Reduction at Silver from a Local Perspective. ACS Catal. 2021;11:14521–32. doi:10.1021/acscatal.1c04791

146. King AJ, Bui JC, Weber AZ, Bell AT. Revealing the Role of the Electrical Double Layer in Electrochemical CO2 Reduction. ACS Catal. 2025;15:14588–600. doi:10.1021/acscatal.5c03725

147. Bui JC, Lees EW, Pant LM, Zenyuk IV, Bell AT, Weber AZ. Continuum Modeling of Porous Electrodes for Electrochemical Synthesis. Chem Rev. 2022;122:11022–84. doi:10.1021/acs.chemrev.1c00901

148. Lees EW, Bui JC, Romiluyi O, Bell AT, Weber AZ. Exploring CO2 reduction and crossover in membrane electrode assemblies. Nat Chem Eng. 2024;1:340–53. doi:10.1038/s44286-024-00062-0

149. Singh DK, Ganesan V, Yadav DK, Yadav M. Metal (Mn, Fe, Co, Ni, Cu, and Zn) Phthalocyanine-Immobilized Mesoporous Carbon Nitride Materials as Durable Electrode Modifiers for the Oxygen Reduction Reaction. Langmuir. 2020;36:12202–12. doi:10.1021/acs.langmuir.0c01822

150. Wan Q, Liu Y, Ke C, Zhang Y, Jiang W, Qu Y, et al. Insight on Performance Degradation of Phthalocyanine Cobalt-Based Gas Diffusion Cathode for Carbon Dioxide Electrochemical Reduction. ACS Sustainable Chem Eng. 2021;9:17214–20. doi:10.1021/acssuschemeng.1c07158

View Article Online
DOI: 10.1039/D6EY00122J

No primary research results, software or code have been included and no new data were generated or analyzed as part of this review.